Geochimica et Cosmochimica Acta 384 (2024) 194–212

Contents lists available at ScienceDirect

Geochimica et Cosmochimica Acta

journal homepage: www.elsevier.com/locate/gca

Experimental constraints on barium isotope fractionation during adsorption–desorption reactions: Implications for weathering and erosion tracer applications

Alasdair C.G. Knight [a,*], Edward T. Tipper [a], Harold J. Bradbury [b], Alexandra V. Turchyn [a], Christoff Andermann [c,d], Heye Freymuth [a], Tim Elliott [e], Luke Bridgestock [a,f]

[a] Department of Earth Sciences, University of Cambridge, Cambridge, CB2 3EQ, Cambridgeshire, UK
[b] Department of Earth, Ocean and Atmospheric Sciences, University of British Columbia, Vancouver, British Columbia, Canada
[c] Géosciences Rennes, Université de Rennes, CNRS, UMR 6118, Rennes, 35042, Brittany, France
[d] Helmholtz Centre Potsdam, GFZ German Research Center for Geosciences, Section 4.6: Geomorphology, Potsdam, 14473, Brandenburg, Germany
[e] School of Earth Sciences, University of Bristol, Bristol, BS8 1RJ, Bristol, UK
[f] School of Earth and Environmental Sciences, University of St Andrews, St Andrews, KY16 9TS, Fife, UK

ARTICLE INFO

Associate editor: Tristan J. Horner

Dataset link: https://doi.org/10.5285/cfa9abd4-1200-47b6-9553-aa1b6e4d9ffd, https://doi.org/10.5281/zenodo.13257704

Keywords:
Adsorption–desorption
Barium isotopes
Weathering
Erosion
Clay minerals
Iron oxyhydroxides

ABSTRACT

Constraining the processes that fractionate barium isotopes is essential for utilising barium isotope ratios as environmental tracers. Barium concentration measurements from soils, rivers, and estuaries demonstrate that adsorption–desorption reactions significantly influence the distribution of fluid–mobile barium at the Earth's surface, potentially driving isotopic fractionation. To quantify the direction and magnitude of isotopic fractionation resulting from these reactions, a riverine and an estuarine series of batch experiments were conducted using environmentally important adsorbent minerals and surface waters. Himalayan river sediment and water samples were used to validate the experimental results.

Adsorption–desorption reactions were found to be rapid, relative to the average transit time of sediment and water in catchments, and largely reversible. The direction and magnitude of isotopic fractionation in the riverine experiment series were consistent with the riverine field samples (preferential adsorption of the lighter isotopes). The reaction rate, reversibility, and magnitude of isotopic fractionation were found to depend primarily on the mineral. Experiments performed with iron oxyhydroxides (goethite and ferrihydrite) resulted in a greater degree of fractionation compared to clay minerals (kaolinite and montmorillonite). Estuarine experiments, designed to simulate sediment passage through a salinity gradient, demonstrated a high degree of reversibility, with 77% to 94% of adsorbed barium desorbed upon the addition of seawater to freshwater-equilibrated clay minerals.

The results of the estuarine experiments suggest that barium isotope ratios measured in marine paleo-archives (*e.g.*, corals) will reflect both the adsorbed and dissolved freshwater barium inputs to the ocean. The combined findings of this study indicate that the chemical and isotopic behaviour of barium differs from more conventional group 1 and 2 metal isotope systems due to a significant proportion of barium released from bedrock dissolution partitioning to mineral surfaces, rapid reaction rates between fluid–mobile phases, and a high degree of reaction reversibility. Consequently, riverine barium isotope ratios are likely to provide unique insights into the complex array of terrestrial weathering and erosion processes that sustain life on Earth.

1. Introduction

Life on Earth is sustained by a complex system of physical and chemical processes that operate within the *Critical Zone*—the dynamic interface between the lithosphere and the atmosphere (Brantley et al., 2007). Stable metal isotope ratios have emerged as important tools for tracing and understanding the temporal and spatial relationships between Critical Zone processes. Stable barium isotope ratios have been successfully used to provide insights into the marine cycling of barium and the associated organic carbon cycle (Bates et al., 2017; Horner et al., 2017; Hsieh and Henderson, 2017; Bridgestock et al., 2018, 2021). Moreover, there is a growing body of research employing barium isotopes to trace terrestrial Critical Zone processes, including:

* Corresponding author.
E-mail address: acgk2@cam.ac.uk (A.C.G. Knight).

https://doi.org/10.1016/j.gca.2024.08.016
Received 27 March 2024; Accepted 22 August 2024
Available online 30 August 2024

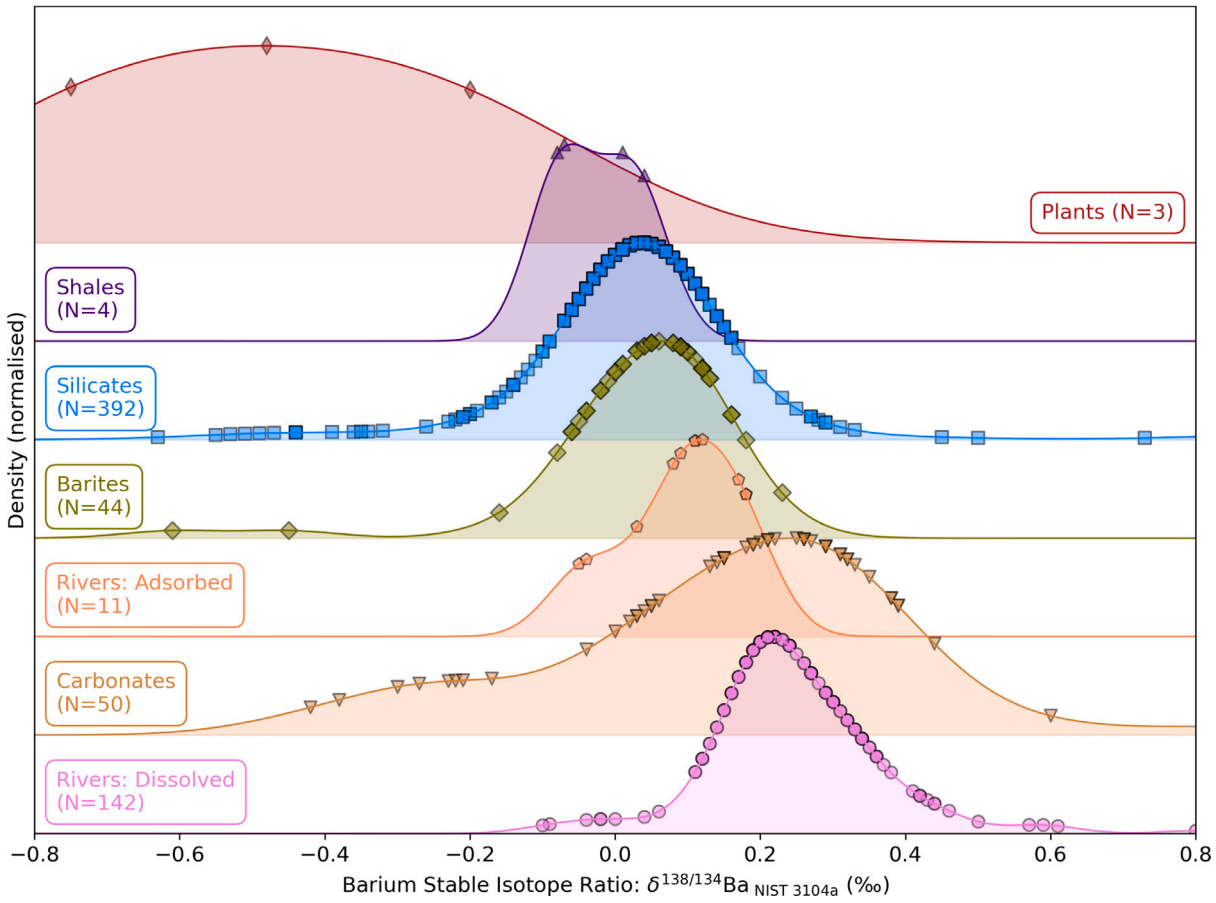

Fig. 1. Stable barium isotope ratios of Critical Zone field samples, expressed relative to the NIST 3104a standard reference material in parts per thousand (‰). The distribution is plotted using a kernel density estimate with a bandwidth of 0.5. The number of observations is indicated in brackets. Data sources include: the dissolved riverine phase (Gou et al., 2020; Cao et al., 2020; Charbonnier et al., 2020, 2022; Tieman et al., 2020; this study), the adsorbed riverine phase (this study), plants (Bullen and Chadwick, 2016), silicates (Bullen and Chadwick, 2016; Nielsen et al., 2018; Nan et al., 2022; Wu et al., 2020; Deng et al., 2021; Nan et al., 2018; Huang et al., 2021; Zhao et al., 2021; Nielsen et al., 2020; Nan et al., 2015; Li et al., 2020), carbonates (Wei et al., 2021), barite (Crockford et al., 2019; von Allmen et al., 2010), and shales (Charbonnier et al., 2020).

nutrient cycling (Charbonnier et al., 2020); chemical weathering (Gong et al., 2020; Charbonnier et al., 2022); riverine temporal dynamics (Gou et al., 2020); and the contributions of riverine inputs to the ocean (Yu et al., 2022).

In freshwater aquatic environments and regolith, fluid–mobile barium (both adsorbed and dissolved) is preferentially partitioned into the adsorbed phase relative to other major alkali and alkaline earth elements. For instance, more than two-thirds of the fluid–mobile barium transported annually by Himalayan rivers was found in the adsorbed phase, compared to just 11% of calcium and strontium, and less than 6% of potassium, magnesium, and sodium (Knight et al., 2024). The adsorbed-to-dissolved barium concentration ratio of Hawaiian soils was also found to be three times higher than that of calcium and strontium (Bullen and Chadwick, 2016). Furthermore, between 20 and 75% of the dissolved barium input to the oceans is estimated to be derived from the surfaces of riverine suspended sediment (Bridgestock et al., 2021). Therefore, adsorption–desorption reactions could be a significant driver of barium isotope fractionation in the Critical Zone, depending on the associated magnitude of fractionation.

Despite the crucial role of adsorption–desorption reactions in controlling the phase distribution of barium at the Earth's surface, the magnitude, direction, and nature of isotopic fractionation between surface waters and common environmental mineral adsorbents remain poorly constrained. This uncertainty has led to ambiguity in the interpretation of field measurements. For instance, both biological uptake (Charbonnier et al., 2020) and adsorption–desorption reactions (Gou et al., 2020) have been proposed as processes responsible for the enrichment of heavy barium isotopes in the dissolved riverine phase relative to the underlying bedrock (Fig. 1).

To better understand the fractionation of stable barium isotopes resulting from adsorption–desorption in freshwater environments, a series of riverine batch experiments were conducted using freshwater analogues (groundwater and river waters) and common environmental mineral adsorbents (clays and iron oxyhydroxides). This experiment series had three main objectives:

1. To quantify the magnitude and direction of barium isotope fractionation associated with different minerals.
2. To determine the reversibility of the reactions.
3. To test if reactions reach chemical and isotopic equilibrium on a timescale relevant to river systems.

To provide a comparison with the laboratory experiments, suspended sediment and water samples collected from Himalayan tributaries of the Ganges–Brahmaputra river system (specifically the Saptakoshi and Sunkoshi rivers) were analysed for their barium concentrations and stable barium isotope ratios. The samples were chosen to span a significant range in runoff and suspended sediment concentrations.

Adsorption–desorption reactions also impact the transportation and fate of fluid-mobile barium in estuaries. Salinity-driven desorption of barium from the surfaces of freshwater-derived suspended sediment occurs in both surface and subterranean estuaries (Li and Chan, 1979; Coffey et al., 1997; Sanders et al., 2012). Quantifying the proportion of barium desorbed, and the associated isotopic fractionation, is vital for developing tracers of terrestrial water and sediment exports to the

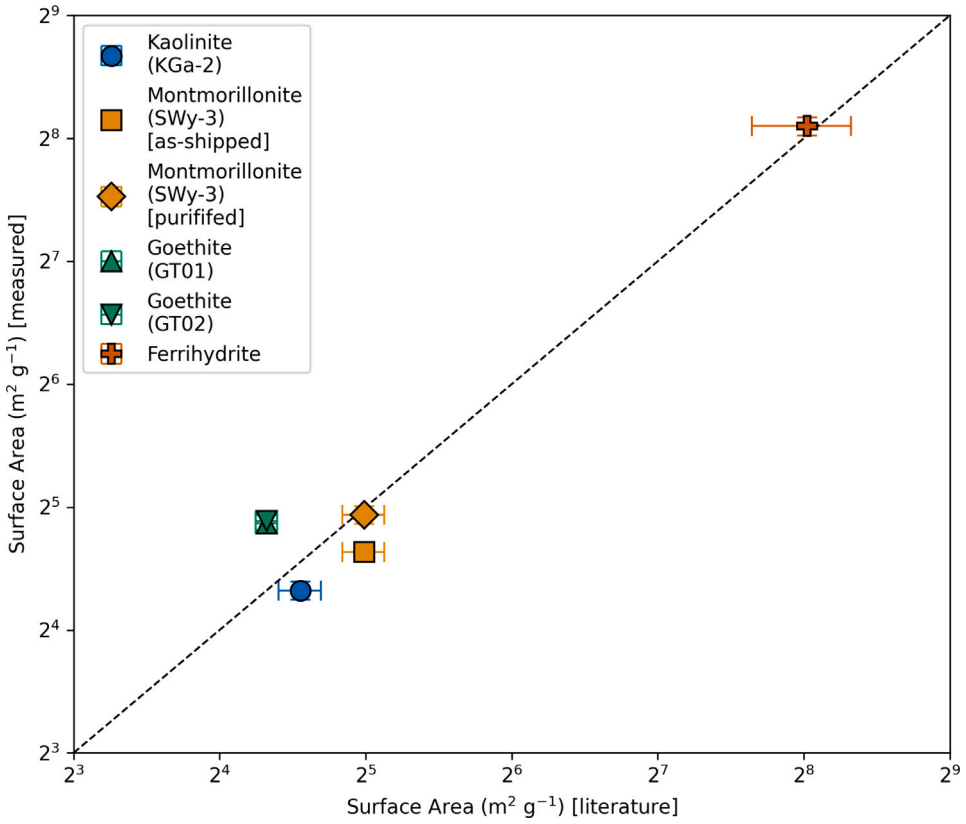

Fig. 2. Experiment mineral surface areas. Surface area measurements are determined from N_2 adsorption experiment isotherms using the BET model. Literature surface area estimates are quoted from (Schwertmann and Cornell, 2008) for goethite and ferrihydrite, and Martin (1980) for kaolinite (KGa-2) and montmorillonite (SWy–2). Kaolinite (KGa-2) and montmorillonite (SWy–2) were degassed at 250 °C. Goethite and ferrihydrite were degassed at 120 °C.

ocean using marine paleo-archives (Hsieh et al., 2022; Yu et al., 2022). To address this, an estuarine series was conducted to replicate the transit of sediment through estuaries across a salinity gradient. This series had two objectives:

1. To determine the proportion of barium desorbed from sediment during estuarine transit.
2. To quantify the magnitude and direction of barium isotope fractionation associated with the desorption process.

Through a combination of experiment series and field samples, a robust quantification of the magnitude and direction of barium isotope fractionation resulting from adsorption–desorption reactions between surface waters and minerals has been made. This advancement enables further exploration of the utility of barium isotopes as tracers of terrestrial Critical Zone processes.

2. Materials and methods

2.1. Materials

2.1.1. Environmentally-relevant mineral adsorbents

Clay minerals are important adsorbents at Earth's surface due to their ubiquity and capacity to adsorb cations (Ito and Wagai, 2017; Sposito et al., 1999). Two well-characterised, high-purity reference samples of kaolinite (KGa-2) and montmorillonite (SWy-2) were purchased from the Clay Minerals Society Source Clays project (Moll, 2001; Schroeder, 2018). The montmorillonite sample (as-shipped) was further purified to remove quartz and feldspar (S.1; Moll, 2001).

Two iron oxyhydroxide minerals, goethite and ferrihydrite, were also selected for this study due to their ubiquity and ability to adsorb metals (Faivre, 2016). The surface charge properties of iron oxyhydroxides differ from clay minerals, resulting in different adsorbative behaviours that vary with environmental variables, particularly pH (Sposito et al., 1999; Faivre, 2016). Both iron oxyhydroxides were synthesised following the methods of Schwertmann and Cornell, 2008 (S.2).

Mineral purity analyses were conducted using powder X-ray diffraction (XRD) to verify that the correct iron oxyhydroxide minerals had been synthesised, and to identify the presence of any significant impurities that could have affected the experiments through dissolution or competitive adsorption (S.3). Mineral surface areas were quantified using the Brunauer–Emmett–Teller (BET) model and nitrogen gas (N_2) adsorption experiments (S.4; Fig. 2). The expected crystal morphology of goethite was confirmed using scanning electron microscope (SEM) images (acicular and elongated; Schwertmann and Cornell, 2008; S.4 C). The other minerals were too small (<1 μm) to easily identify individual crystals with SEM images, which is consistent with their large surface-area-to-volume ratios (S.5).

2.1.2. Waters

Two terrestrial waters and one seawater sample were selected for the experiments to represent a broad range of natural surface water chemistries (Tab. S.1). A sample of Buxton® still mineral water (BU100) was used as a proxy for a high ionic strength river or groundwater (Fig. 3). BU100 was found to be oversaturated with respect to several mineral phases, including barite, with a saturation index (SI_{barite}) ranging from 0.12 to 0.31. Barite precipitation, dissolution, and equilibrium lattice ion-exchange reactions have been shown to be important drivers of barium isotope fractionation in marine environments (Middleton et al., 2023a,b; van Zuilen et al., 2023). To avoid isotopic fractionation caused by mineral precipitation, a second mineral water sample (HS50) was diluted with ultrapure water to achieve undersaturation with respect to common mineral precipitates (SI_{barite} = −0.65 to −0.44). Seawater (SWH) was collected at a distance of 10 meters from the shoreline

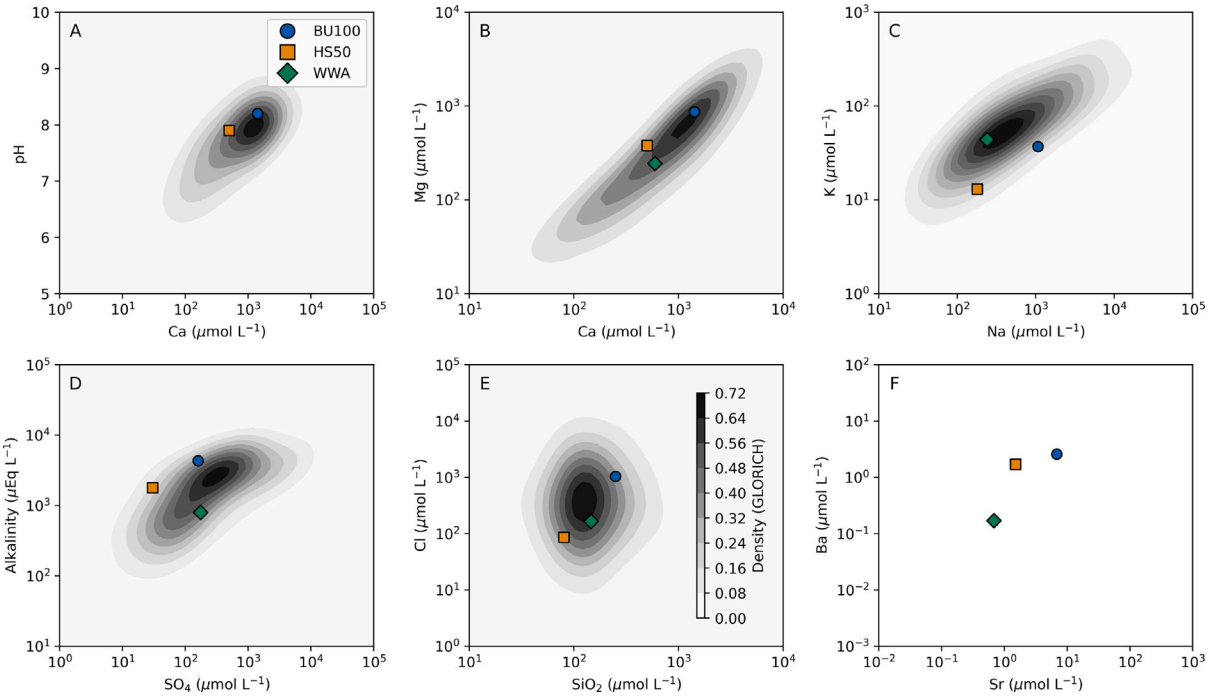

Fig. 3. Comparison of the dissolved chemistry of terrestrial experimental waters (BU100: blue circles, HS50: orange squares) with global river chemistry. Dissolved element concentrations are presented in units of μmol L^{-1}. Discharge-weighted average (WWA) element concentration estimates for large rivers are represented by green diamonds. Major riverine element concentrations (Ca, K, Mg, Na, SO_4, HCO_3, SiO_2) are sourced from the world discharge–weighted average (WWA) of Meybeck (2003). Riverine trace element concentrations are from Gaillardet et al. (2003). Grey contours illustrate the bivariate kernel density estimate (KDE) of the GLORICH database (Hartmann et al., 2019). pH measurements were conducted using a Thermo Fisher Scientific Orion Star A211 Benchtop pH meter at the University of Cambridge.

at Hunstanton, UK, and filtered through 0.22 μm polyethersulfone (PES) membrane filters in-situ to remove suspended particulate matter.

2.1.3. Field samples

River water and suspended sediment samples were analysed for their sediment-adsorbed and dissolved barium concentrations and barium isotope ratios to facilitate a comparison between the laboratory and field samples. A total of 12 samples were selected from a larger time series, collected between 2015 and 2018 from the Sunkoshi and Saptakoshi rivers, to span a large range in runoff and suspended sediment concentrations. These rivers are major contributors of sediment and water to the Ganges–Brahmaputra river system—the second largest point source of sediment to the ocean (Andermann et al., 2012; Milliman and Farnsworth, 2013).

Samples were collected from the upper meter of the water column using USGS DH-48 depth-integrating fish samplers lowered from bridges. To separate the suspended sediment from the water, in-situ filtration was performed using 0.22 μm polyethersulfone (PES) membrane filters. Sediment samples were scraped from the filters to avoid perturbing the chemical composition of the adsorbed phase. The procedures for adsorbed phase extractions, barium concentration measurements, and isotope ratio analyses followed the same protocols as those used in the laboratory experiments.

2.2. Experiment series

2.2.1. Riverine

The Riverine Series was conducted to investigate the fractionation of barium stable isotopes during adsorption–desorption reactions in freshwater environments. This series included experiments with two types of freshwater (HS50 and BU100) and four different minerals (kaolinite, montmorillonite, goethite, and ferrihydrite). The experiments were organised into two subseries (see Fig. 4).

The Partitioning Subseries aimed to assess how the mineral-to-water ratio affected the distribution of barium between the adsorbed and dissolved phases. The clay minerals were sourced from natural deposits and therefore required cleaning prior to the start of the experiments to remove adsorbed barium (Section 2.3.1). Iron oxyhydroxides were synthesised in the laboratory from high-purity reagents and therefore did not need to be cleaned (Section 2.1.1). The impact of the cleaning procedure on the chemical and isotopic behaviour of barium was assessed by performing iron oxyhydroxide experiments with and without the pre-experiment treatment step. Treated and untreated minerals were added to waters at varying mineral concentrations: kaolinite (10 g L^{-1} to 100 g L^{-1}); montmorillonite (0.5 g L^{-1} to 100 g L^{-1}); goethite (5 g L^{-1} to 150 g L^{-1}); and ferrihydrite (0.3 g L^{-1} to 100 g L^{-1}). The reaction duration was kept constant for all experiments in this subseries (2000 min). To maintain thorough mixing of the minerals and water, shaking and ultrasonication were employed (Section 2.3.2). Reactions were terminated following centrifugation and phase separation. The Partitioning Subseries was crucial for subsequent experiments to ensure that the target mass of barium required for a reliable barium isotope measurement was present in the water and leachate (200 ng).

The Kinetic Subseries was designed to examine the effect of reaction duration on the partitioning of barium between the adsorbed and dissolved phases, as well as on the fractionation of barium isotopes. Reaction durations in this subseries ranged from 10 min — the shortest practical time achievable with the batch method — to just over a month (50 000 min). All experiments in this subseries utilised pre—cleaned minerals treated with 1.0 M NH_4Cl and constant mineral-to-water ratios were used: kaolinite (53 g L^{-1}), montmorillonite (1.7 g L^{-1}), goethite (75 g L^{-1}), and ferrihydrite (4 g L^{-1}). Continual pH logging at 3 s intervals was conducted in a replicate experiment to gain additional insights into reaction kinetics (S.7). The findings from this subseries were used to evaluate reaction kinetics and reversibility, aiding in the assessment of the likelihood of reaching chemical and isotopic equilibrium in field samples. In the absence of direct measurements of forward and backward reaction rates, equilibrium was inferred from the point at which the concentrations or isotope ratios in the dissolved and

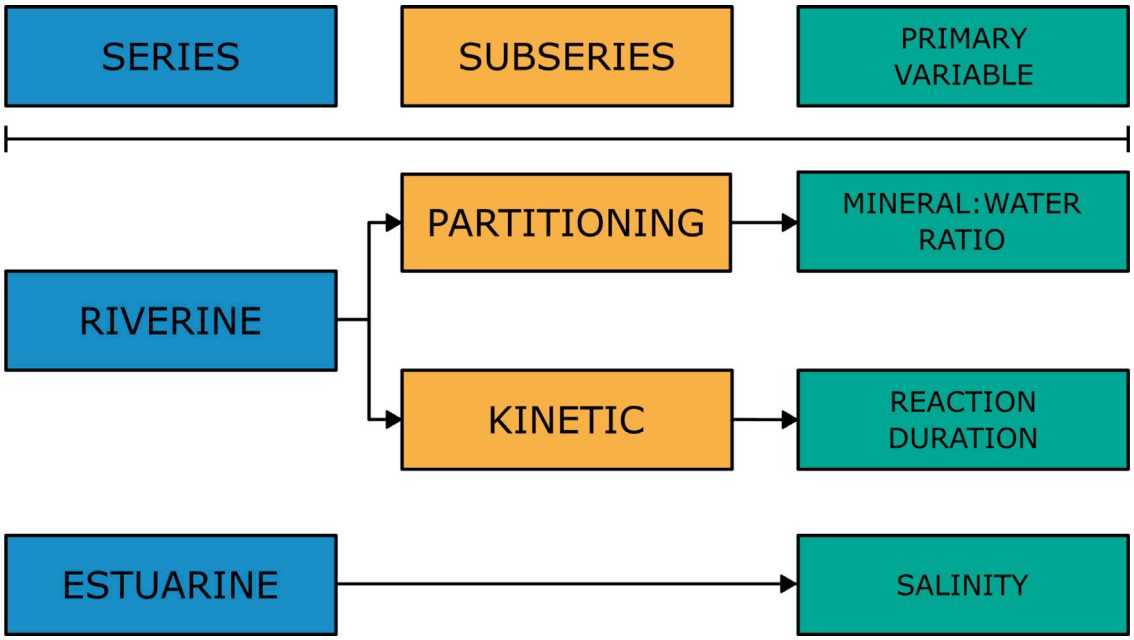

Fig. 4. Overview of the batch experiment series. The riverine series was divided into two subseries: (1) the Partitioning Subseries, which explored variable mineral-to-water ratios to assess how different mineral concentrations affect the fractionation of barium stable isotopes, and (2) the Kinetic Subseries, which investigated the influence of varying reaction durations on barium isotope fractionation.

adsorbed phases remained stable within analytical uncertainty, referred to as steady-state.

After completing each batch experiment, the reacted water and mineral phases were separated via centrifugation and filtration. Adsorbed barium was displaced from the mineral surfaces following the procedure outlined in Section 2.3.3, followed by barium concentration and isotope ratio analyses of both fluid-mobile phases (Section 2.3.4 & Section 2.3.6).

2.2.2. Estuarine

The estuarine experiments followed the same initial procedures as the riverine series: pre-cleaning of clays, equilibration with a river water analogue, and separation of the water and clay. Seawater was then added to simulate the mixing of river–water-equilibrated minerals with saline fluids. Unlike the riverine series, where the mineral concentration was varied, the clay concentration was kept constant throughout this series. Following the addition and removal of seawater, half of the experiments were re-equilibrated with an equal volume of the river water analogue used in the initial equilibration. All stages of the Estuarine Series were conducted with a constant reaction duration of 10 000 min, based on a conservative estimate for achieving chemical equilibrium between the clay-adsorbed and dissolved phases. The processes for the separation of phases, measurement of barium concentrations, and determination of barium isotope ratios in the Estuarine Series were identical to those used in the Riverine Series.

2.3. Methods

All experiments were conducted in clean laboratories specifically designed for trace metal isotope analyses at the Department of Earth Sciences, University of Cambridge. The experiments were performed under controlled conditions at 20 °C and 1 atm. Reagents were maintained at room temperature unless otherwise specified. Polypropylene (PP) centrifuge tubes and polytetrafluoroethylene (PTFE) beakers were acid-cleaned with single-distilled HNO_3 and thoroughly rinsed with ultrapure water to prevent contamination.

2.3.1. Displacement of pre-existing adsorbed barium from adsorbents

The pre-experiment cleaning of clay minerals was necessary because the naturally adsorbed barium concentrations on the clays represented up to 950% of the total barium added from the waters (average 70%). To address this, repeated additions of 1.0 M NH_4Cl (Puratronic™, 99.999% trace metal basis) were carried out to displace the pre-adsorbed Ba^{2+} from the surfaces of the clay minerals in exchange for NH_4^+ ions:

$$2\,NH_4^+ + Ba{-}S_2 \xrightarrow{\text{desorption}} 2\,NH_4{-}S + Ba^{2+} \quad (1)$$

Where S denotes a negatively charged surface site.

The minerals were first placed into polypropylene centrifuge tubes, and 1.0 M NH_4Cl was added at the following concentrations: kaolinite at 250 g L^{-1}, montmorillonite at 25 g L^{-1}, goethite at 150 g L^{-1}, and ferrihydrite at 25 g L^{-1}. These concentrations were initially based on literature estimates of the cation exchange capacity (CEC) of each mineral, but were adjusted to minimise the volume of NH_4Cl needed for the near-complete desorption of barium (Fig. S.7). The mixture of minerals and NH_4Cl was then shaken, followed by ultrasonication in an ultrapure water bath for 30 min. The tubes were then placed on a shaker table for 2 h. After mixing, the adsorbent was separated from the supernatant by centrifugation at 3100 g for 30 min. The supernatant was transferred to separate polypropylene centrifuge tubes using a pipette and immediately filtered through 0.22 µm PES filters. The process was repeated three times with fresh 1.0 M NH_4Cl to maximise the extraction of reversibly adsorbed barium and minimise the potential reagent blank. Three extractions were selected as the optimal number based on pre-experiment tests (S.8). Finally, the treated minerals were washed three times in ultrapure water to remove any residual NH_4Cl.

2.3.2. Mineral-Water reactions

Experiment waters were added to the minerals in polypropylene centrifuge tubes. Several procedures were employed to ensure thorough mixing of the mineral and water throughout the experiment, depending on the duration of the experiment (10 min to 50 000 min). For experiments lasting less than 40 min, manual shaking was sufficient to keep the mineral and water in suspension, allowing adequate time for centrifugation. For experiments exceeding 40 min, centrifuge tubes

were ultrasonicated in an ultrapure water bath for 20 min, then placed on a shaker table for the remainder of the reaction period to ensure continuous mixing. After the designated reaction time, the supernatant and adsorbent were separated by centrifugation at 3100 g for 30 min. The supernatants were then immediately filtered through 0.22 µm PES membrane filters. The end of the reaction was marked by the physical separation of the water and mineral phases. Reacted waters were transferred to clean polypropylene centrifuge tubes for further analysis.

2.3.3. Extraction of the adsorbed phase

The displacement of adsorbed barium cations from mineral surfaces was achieved following a method identical to the initial cleaning procedure outlined in Section 2.3.1. This occurred immediately following the separation of the water and the mineral. All water and leachates were refrigerated at 5 °C prior to analysis.

2.3.4. Determination of element concentrations

Element concentrations were measured via inductively coupled plasma optical emission spectroscopy (ICP-OES) on an Agilent 5100 at the Department of Earth Sciences, University of Cambridge. Synthetic calibration lines, produced with certified standards, were used to calibrate element concentrations. Samples, external standards, and calibration lines were matrix-matched prior to analyses. To prevent pressure-drift during measurement sessions, samples were diluted to 0.04 M NH_4Cl and an argon gas humidifier was employed. The maximum uncertainty for barium concentration measurements was 7% based on repeated analyses of two externally verified surface water standards (SPS-SW2 and SLRS-6). Barium concentrations were independently determined by isotope dilution from thermal ionisation mass spectrometry (TIMS) measurements (Rudge et al., 2009). Repeat analyses of two standard reference materials — NIST 3104a (barium carbonate) and NBS 127 (barite) — yielded an uncertainty of 2% (2σ). Barium concentrations determined via TIMS were preferentially used when available. Agreement between the ICP–OES and TIMS measurements was typically within 8% (Fig. S.8). The accuracy and precision of repeated external standard measurements via ICP-OES for all elements are detailed in Tab. S.2.

2.3.5. Mass distribution ratios

The mass distribution ratio quantifies the partitioning of barium between the adsorbed and dissolved phases, accounting for varying mineral-to-water ratios. Reversible distribution ratios were calculated using the concentration of barium in the adsorbed phase [Ba_{ad}; mol kg^{-1}] and the dissolved phase [Ba_{diss}; mol L^{-1}]:

$$K_{D[r]} = \frac{[Ba_{ad}]}{[Ba_{diss}]} \tag{2}$$

Irreversible distribution ratios were also determined using the difference in barium concentration between the initial experiment water [$Ba_{e.w.}$; mol L^{-1}] and the remaining water:

$$K_{D[ir]} = \frac{[Ba_{e.w.}] - [Ba_{diss}]}{[Ba_{diss}]} \tag{3}$$

2.3.6. Barium isotope measurements

The barium isotopic composition of the dissolved and adsorbed phases were determined via TIMS on a Thermo Fischer Scientific TRITON Plus instrument at the Department of Earth Sciences, University of Cambridge. Barium isotope ratio measurements (smp) were normalised to the isotope ratio of the NIST 3104a standard reference material (std):

$$\delta^{138}Ba_{smp}(‰) = \left(\frac{\left(^{138}Ba/^{134}Ba\right)_{smp}}{\left(^{138}Ba/^{134}Ba\right)_{std}} - 1 \right) \times 10^3 \tag{4}$$

Experiment samples are provided relative to the barium isotope ratio of the initial experiment water used (e.w.), to allow for a straightforward comparison between experiments using differing water chemistries:

$$\delta^{138}Ba^{*} = \delta^{138}Ba_{smp} - \delta^{138}Ba_{e.w.} \tag{5}$$

A target mass of 200 ng of barium was selected for a high-precision isotope ratio measurement, based on the method of Bridgestock et al. (2021). Each sample aliquot was transferred to a clean polytetrafluoroethylene (PTFE) beaker, and a known quantity of double-spike solution was added to correct for mass-dependent fractionation during the chemical purification and TIMS analysis stages (see S.10.1 for mixing and calibration details). The samples were shaken and refluxed on a hot plate at 80 °C for 24 h to equilibrate the sample-spike mixture. For seawater samples, the calcite co-precipitation method of Foster et al. (2004) was employed to enhance the barium-to-high-concentration-element (Na, Mg, K) ratio before column chromatography. To remove NH_4Cl — which was discovered to prevent the effective ionisation and evaporation of BaCl during TIMS — the samples were evaporated, treated with 1 mL of aqua regia, and refluxed on a hot plate at 140 °C for 24 h. This was followed by evaporation to dry salts on a hot plate at 80 °C. Two additional rounds of aqua regia addition and evaporation were then performed. Finally, single-distilled 3.0 M HCl (1 mL) was used to re-dissolve the sample for cation exchange column chromatography.

A two-stage ion exchange chromatography column method, adapted from Hsieh and Henderson (2017), was used to separate barium from matrix cations (see S.10.2 for sample preparation details). Results from column calibrations performed using the HS50 river water analogue are shown in Fig. S.10. After chromatography, samples were evaporated, dissolved, and refluxed in ultrapure 9.8 M H_2O_2 (99.9999% trace metal basis; Sigma Aldrich) for 24 h to oxidise organic matter, then dried and loaded onto zone-refined rhenium filaments (99.999% purity; H CROSS) in 1 µL of single-distilled 3.0 M HCl. Details of the isotope measurement protocols are provided in S.10.3.

The combined chromatography and TIMS procedural blank was 0.07 ± 0.06 ng ($\mu \pm 2\sigma$, $N = 6$), representing <1% of the processed sample mass (200 ng). The measured 1.0 M NH_4Cl blank was 3.23 ± 0.02 ng mL^{-1} ($\mu \pm 2SE$), contributing a maximum of 4% to the total experimental barium. Repeated measurements of two standard reference materials (NIST 3104a and NBS 127) over three years were used to determine the long-term accuracy and precision of the method, with a minimum uncertainty of 0.03 ‰ for all isotopic measurements (NBS 127 $\delta^{138}Ba = -0.29 \pm 0.03$ ‰; $\mu \pm 2\sigma$, $N = 31$). The method was further validated via measurements of other certified reference materials (see Fig. S.11). Additional details on the method's accuracy and precision are provided in S.10.4.

2.3.7. Quantifying the direction, magnitude and nature of isotopic fractionation

The partitioning of ^{138}Ba and ^{134}Ba between the adsorbed (ad) and dissolved (diss) phases can be expressed by an isotopic fractionation factor (α):

$$\alpha_{ad-diss} = \frac{R_{ad}}{R_{diss}} \tag{6}$$

Where R is the ^{138}Ba to ^{134}Ba ratio. The magnitude of fractionation is given by the absolute difference between the measured value of α and 1. The direction of isotopic fractionation is indicated by whether α is greater than or less than 1. Specifically, if α is less than 1 in this study, this signifies that the adsorbed phase was enriched in the lighter isotope (^{134}Ba) relative to the dissolved phase, which was enriched in the heavier isotope (^{138}Ba). Closed-system equilibrium and Rayleigh isotopic fractionation models were applied to the post-experiment dissolved and adsorbed isotope ratios as a function of the proportion of barium adsorbed, to determine if the isotopic fractionation could be modelled by standard isotopic fractionation models. Non-linear least squares regression was used to find the optimal fractionation factor (S.12).

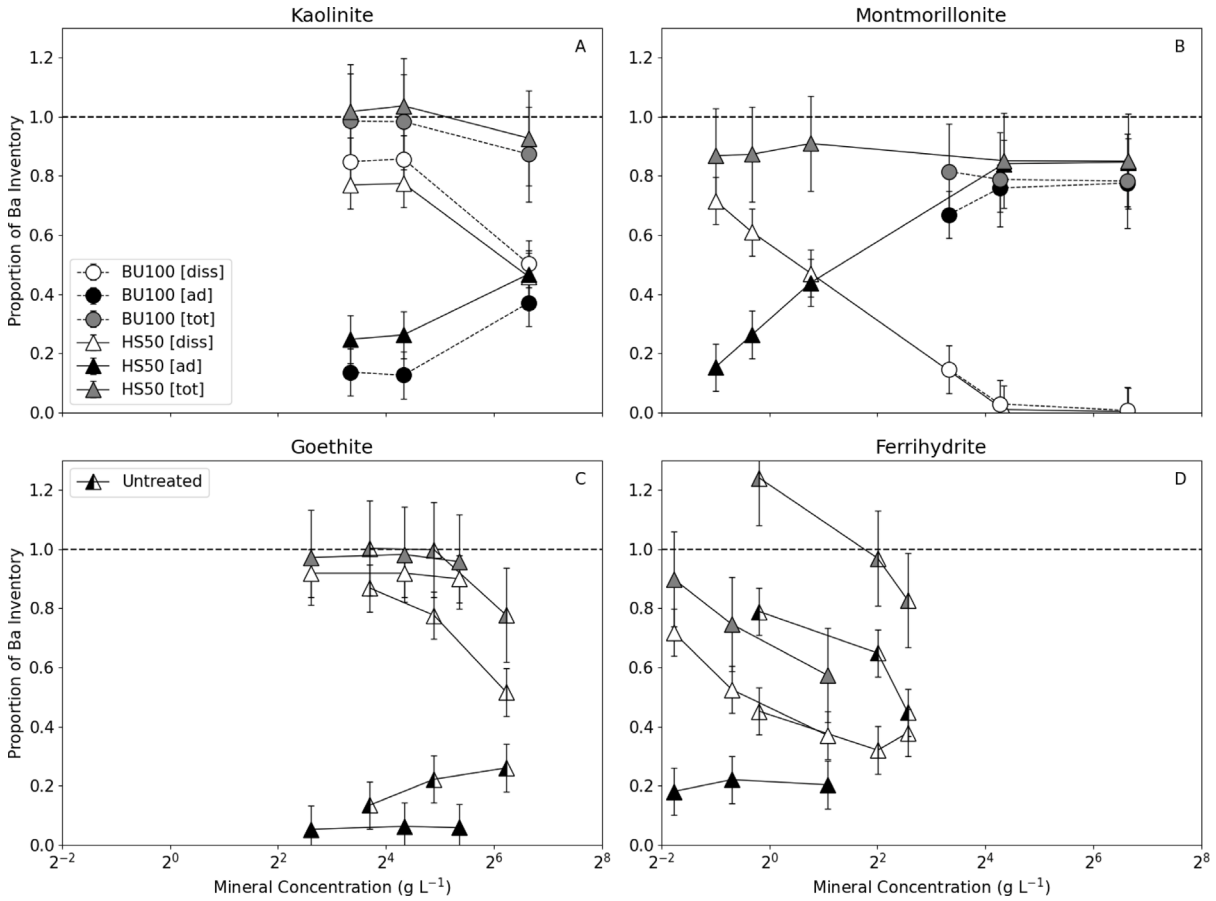

Fig. 5. Partitioning of barium between dissolved and adsorbed (leached) phases as a function of mineral concentration. Marker shapes indicate water chemistries: BU100 (circles) and HS50 (triangles). Marker face colours denote phases: white for dissolved, black for adsorbed, and grey for total fluid-mobile. Error bars display twice the standard deviation of standard measurements. Black dashed horizontal lines indicate complete (100%) recovery of the initial barium. Experiments without initial NH_4Cl cleaning (untreated) are denoted by left-filled markers.

3. Results

3.1. Riverine series

3.1.1. Barium concentrations

Partitioning subseries

The partitioning of barium between the adsorbed and dissolved phases in the Partitioning Subseries varied with the mineral-to-water ratio, the mineral type, and use of NH_4Cl to clean the minerals (Fig. 5).

A positive relationship was observed between the clay-to-water ratio and the adsorbed barium proportion, whereas a negative relationship was observed between the clay-to-water ratio and the dissolved barium proportion (Fig. 5 A–B). The overall recovery of barium, defined as the sum of adsorbed and dissolved barium masses relative to the initial mass added, did not vary significantly with the clay concentration: kaolinite experiments achieved complete barium recovery (Fig. 5 A), while montmorillonite experiments showed an average recovery of 84% (Fig. 5 B).

In contrast, the relationship between iron oxyhydroxide concentrations and barium phase proportions was more complex and dependent on whether the adsorbent was pre-cleaned with NH_4Cl (Fig. 5 C–D). For treated goethite samples, there was no significant change in the proportions of adsorbed and dissolved barium with increasing concentration (Fig. 5 C). However, untreated goethite experiments showed an increase in the proportion of adsorbed barium and a decrease in the dissolved barium. For ferrihydrite, treated samples exhibited a decrease in the proportion of dissolved barium while the adsorbed barium remained constant (Fig. 5 D). Untreated ferrihydrite samples showed a decrease in the proportion of adsorbed barium with increasing concentration, while the dissolved barium proportion remained stable (Fig. 5 D).

The pre-cleaning procedure with NH_4Cl also influenced the proportion of fluid-mobile barium adsorbed at a given iron–oxyhydroxide-to-water ratio. Untreated iron oxyhydroxides generally adsorbed a greater proportion of barium compared to treated samples (Fig. 5 C–D). Additionally, barium recovery decreased with increasing iron oxyhydroxide concentration, except for treated goethite experiments. Ferrihydrite experiments showed a notable decrease in recovery from approximately 90% at $0.3\,g\,L^{-1}$ to around 60% at $2.2\,g\,L^{-1}$ (Fig. 5 D).

The distribution ratios (K_D) in the Partitioning Subseries of experiments varied significantly depending on the type of mineral used in the experiment (Fig. 6). Montmorillonite exhibited the highest average K_D, with a value of $1370\,L\,kg^{-1}$, followed by ferrihydrite at $750\,L\,kg^{-1}$, kaolinite at $11\,L\,kg^{-1}$, and goethite at $7\,L\,kg^{-1}$. For kaolinite, the K_D values decreased by a factor of 1.8–2.3 as the kaolinite concentration was increased from $10\,g\,L^{-1}$ to $100\,g\,L^{-1}$ (Fig. 6 A). In the case of montmorillonite, the K_D remained relatively constant at an average of $490\,L\,kg^{-1}$ up to a concentration of $10\,g\,L^{-1}$ (Fig. 6 B). Above this concentration, the K_D values rose significantly, exceeding $4000\,L\,kg^{-1}$. For goethite, the K_D values generally decreased with increasing concentration, except for one experiment where this trend did not hold (Fig. 6 C). The majority of ferrihydrite experiments exhibited a similar trend, with a decrease in K_D observed as the ferrihydrite-to-water ratio was increased (Fig. 6 D).

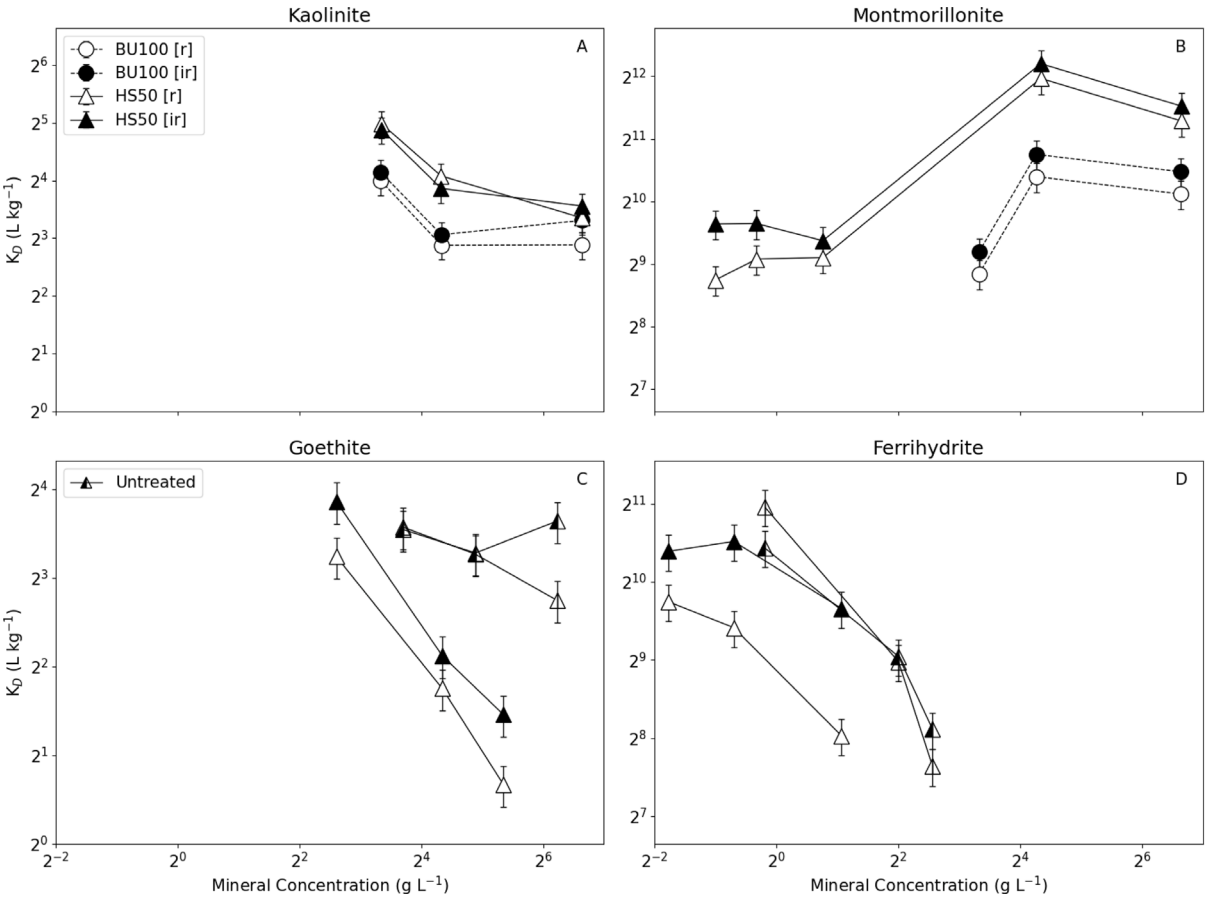

Fig. 6. Distribution ratios (K_D) as a function of adsorbent concentration. Reversible distribution ratios are shown with white markers, and irreversible distribution ratios with black markers. Marker shapes denote water chemistries: BU100 (circles) and HS50 (triangles). Left-filled markers indicate experiments without an initial NH_4Cl cleaning procedure (untreated).

Kinetic subseries

In the Kinetic Subseries, barium recovery was invariant of the reaction duration for experiments involving kaolinite and goethite. Near-complete recovery was achieved with kaolinite (99 ± 3%) and goethite (98 ± 5%), whereas a lower degree of recovery was exhibited for experiments using montmorillonite (80 ± 10%). Experiments performed with ferrihydrite, however, showed a systematic decrease in barium recovery as the reaction duration increased, with a significant drop occurring after 1000 min—reaching approximately 30% recovery at 50 000 min. For reaction durations up to 1000 min, recovery factors for ferrihydrite experiments ranged from 80% to 90%. The proportion of barium recovered remained unaffected by variations in the initial water chemistry.

The reaction duration required to achieve chemical steady-state varied among different minerals and water types. For kaolinite-HS50 experiments, steady-state was reached in ca. 500 min. In contrast, kaolinite-BU100 experiments did not achieve steady-state in either phase. Montmorillonite experiments reached steady-state in 100 min for both waters. Goethite achieved steady-state in 50 min. For ferrihydrite, the phase proportions did not vary significantly between 50 min and 1000 min. However, the concentration of dissolved barium in ferrihydrite experiments decreased substantially after 1000 min, averaging 9% of the total barium added at 50 000 min. The concentration of adsorbed barium in ferrihydrite experiments remained at steady-state after 10 min.

The ability of the minerals to adsorb barium followed the same trend as observed in the partitioning experiments. Montmorillonite had the highest mean distribution ratio (K_D) at 950 L kg^{-1}, followed by ferrihydrite (140 L kg^{-1}), kaolinite (45 L kg^{-1}), and goethite (10 L kg^{-1}). Across all mineral–water pairings, K_D values for the longest reaction duration were greater than the shortest (Fig. 8).

3.1.2. Barium isotope ratios

The direction of isotope fractionation was consistent across all experiments: the adsorbed phase was enriched in the lighter isotope (^{134}Ba), while the dissolved phase was enriched in the heavier isotope (^{138}Ba), relative to the initial barium pool. However, the magnitude of isotopic fractionation, measured as the offset between paired phases, differed among adsorbents. Specifically, clay minerals resulted in a smaller degree of isotope fractionation compared to iron oxyhydroxides (Fig. 14).

Partitioning subseries

A limited subset of samples from the iron oxyhydroxide experiments were analysed for barium isotope ratios as a function of adsorbent concentration (Fig. 10). The relationship between the isotope ratio (δ^{138}Ba) of the fluid-mobile phases and the iron oxyhydroxide concentration varied depending on the use of the pre-treatment procedure with NH_4Cl. A negative correlation was observed between the dissolved phase and the treated goethite-to-water ratio, while a positive correlation was found in the untreated goethite experiments. Similarly, a positive relationship between the isotope ratio of both fluid-mobile phases and the concentration of treated ferrihydrite was observed, with the offset between the phases remaining within analytical uncertainty. No consistent relationship was observed between the dissolved phase and the concentration of untreated ferrihydrite.

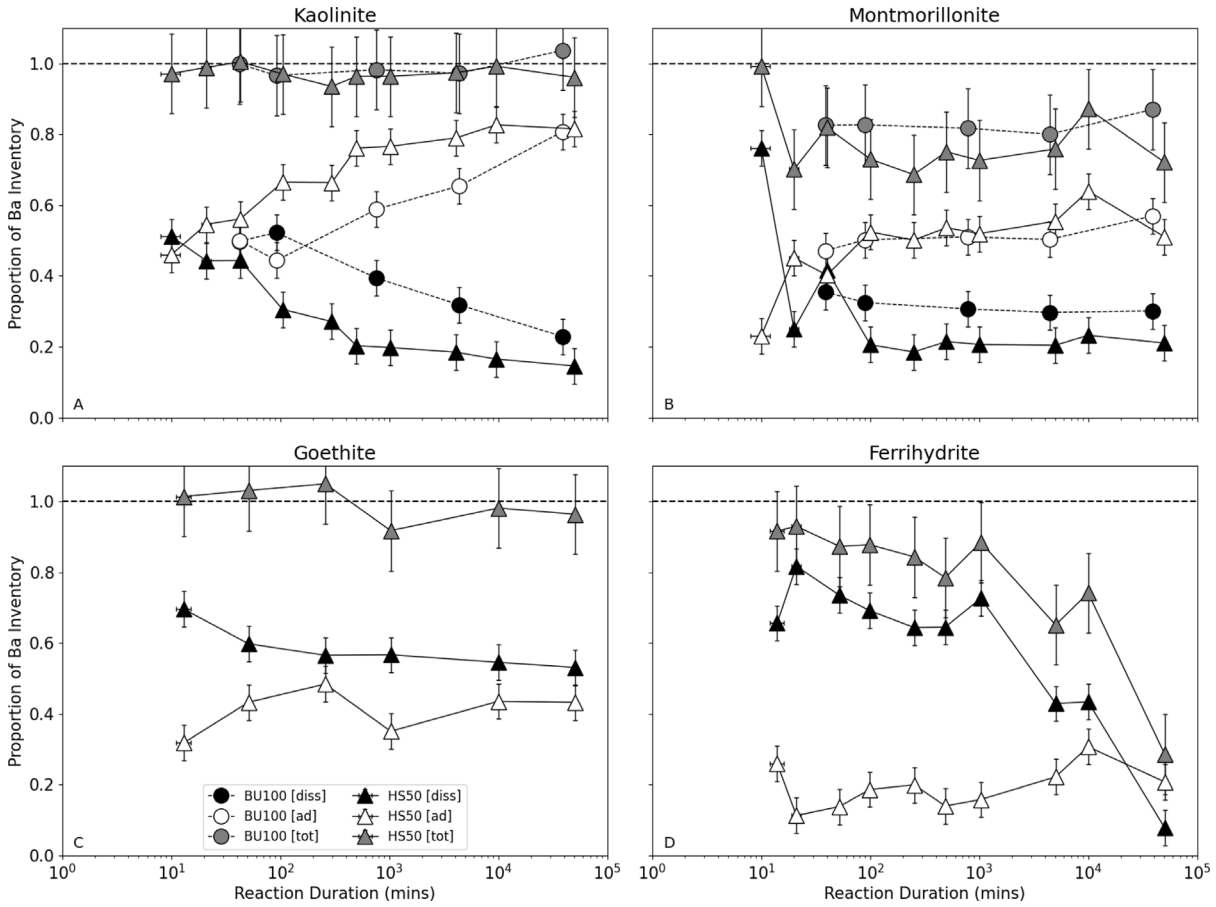

Fig. 7. Proportion of the total experiment barium inventory measured in the dissolved and adsorbed (leached) phases as a function of reaction duration. Marker shapes represent water chemistries: BU100 (circles) and HS50 (triangles). Marker face colours denote different phases: blue (dissolved), orange (adsorbed), and purple (total fluid-mobile). Error bars represent twice the standard deviation of standard measurements. Black dashed horizontal lines indicate complete (100%) recovery of the barium added at the start of the experiment.

Kinetic subseries

The isotopic offsets between the dissolved and adsorbed phases ($\Delta^{138}Ba_{diss-ad}$) were within analytical uncertainty for the majority of kinetic experiments (Fig. 9). Similarly, the isotopic composition of the individual phases ($\delta^{138}Ba$) also generally fell within the same range of uncertainty (Fig. 11). Notable exceptions include: an increase in both the adsorbed and dissolved barium isotope ratios over time in the goethite experiments; and a rise in the dissolved $\delta^{138}Ba^*$ during the final ferrihydrite experiment. The degree of isotope fractionation observed between paired samples remained consistent regardless of the proportion of barium recovered from the experiments (Fig. 12).

3.2. Estuarine series

3.2.1. Barium concentrations

The initial addition of river water (HS50) to clay minerals led to the removal of 49%–59% of the dissolved barium from the water in the kaolinite experiments and 32%–35% in the montmorillonite experiments. When seawater (SWH) was subsequently added to the clay minerals, there was a significant increase in dissolved barium concentrations (Fig. 13 B). A substantial proportion of the dissolved barium removed from HS50 was returned to the seawater (kaolinite = 89 ± 5%, N=2; montmorillonite = 79 ± 5%, N=2), resulting in a 9 to 16-fold increase in the seawater (SWH) barium concentration. The final re-equilibration with river water (HS50) resulted in a slightly smaller proportion of dissolved barium being adsorbed compared to the initial river water equilibration stage (kaolinite = 38%, montmorillonite = 26%).

3.2.2. Barium isotope ratios

During all stages of the Estuarine Series experiments, the adsorbed phase was consistently enriched in the lighter isotope (^{134}Ba), while the remaining dissolved phase was enriched in the heavier isotope (^{138}Ba). The initial addition of the river water analogue, HS50, to montmorillonite and kaolinite caused the barium isotope ratio of the dissolved phases to increase by 0.02–0.04 ‰ and 0.03–0.11 ‰, respectively (Fig. 13 A). The subsequent addition of seawater resulted in barium isotope fractionation in an identical direction to the first step, offsetting the fluid-mobile phases from a binary mixture between barium removed from the river water analogue and the dissolved barium in seawater (Fig. 13 C). In the final river water re-equilibration step, the dissolved phase remained offset from the leached phase by a similar magnitude to that modelled during the initial river water equilibration step ($\Delta^{138}Ba_{diss-ad}$: kaolinite = 0.11 ‰ ; montmorillonite = 0.06 ‰).

3.3. Field samples

The proportion of fluid-mobile barium (the sum of the adsorbed and dissolved barium) in the adsorbed phase in the Himalayan rivers ranged from 14% to 98%, with maximum proportions coinciding with maximum suspended sediment concentrations (SSCs; Fig. 14 A & B). The direction of isotope fractionation in field samples mirrored that observed in all laboratory experiments, with the adsorbed phase enriched in the lighter isotope (^{134}Ba) and the dissolved phase enriched in the heavier isotope (^{138}Ba; Fig. 14 C). Isotope ratios for the fluid-mobile phases also exhibited seasonal variability, with higher ratios in both the adsorbed and dissolved phases during the monsoon and

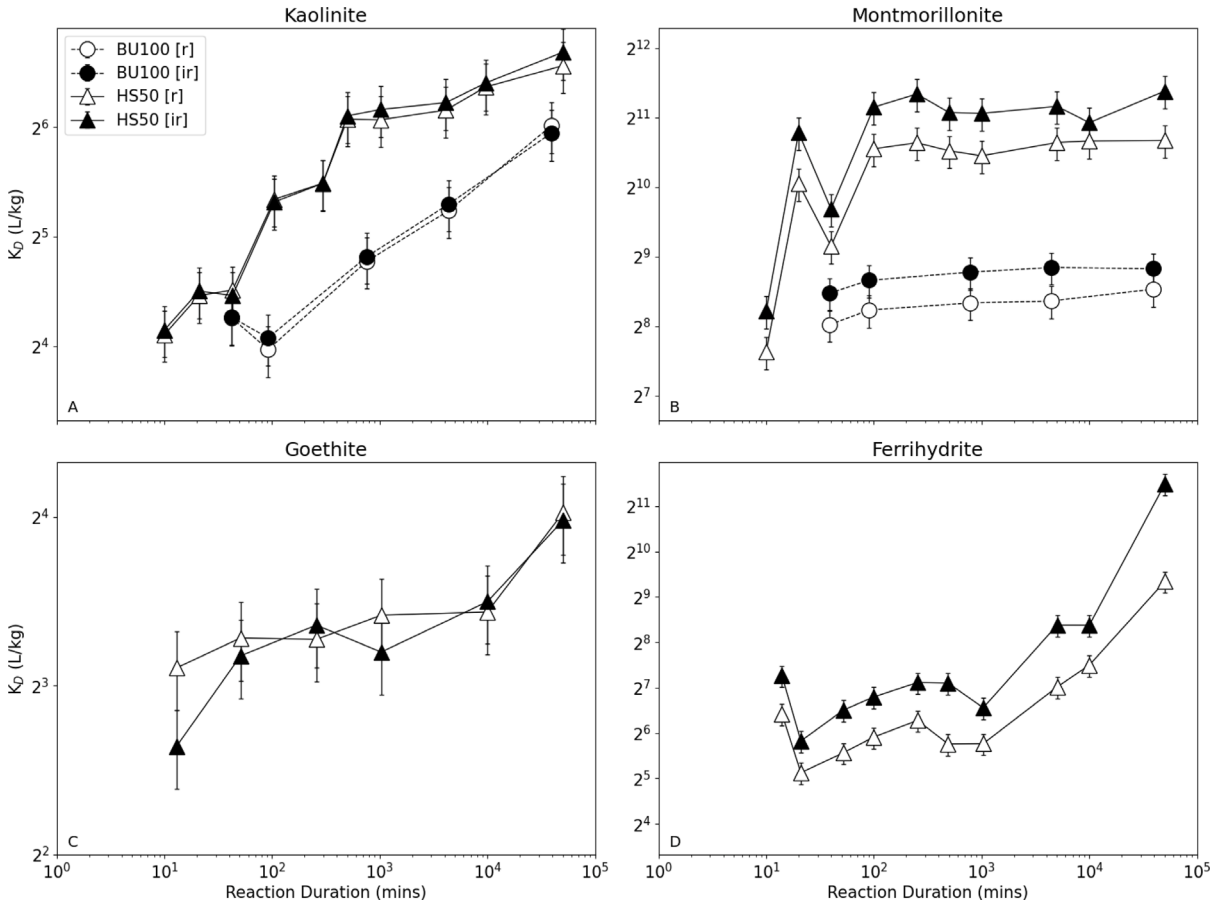

Fig. 8. Distribution ratios (K_D) as a function of reaction duration. Reversible distribution ratios are shown with white markers, and irreversible distribution ratios with black markers. Different water chemistries are indicated by marker shapes: BU100 (circles) and HS50 (triangles). Experiments where an initial NH_4Cl cleaning procedure was not applied (untreated) are shown by left-filled markers.

lower values during the pre- and post-monsoon periods (Fig. 14 C). The offset between the phases for paired samples was consistent with laboratory studies, ranging from 0.01 ‰ to 0.33 ‰, with an average of 0.19 ‰ . In contrast, the distribution ratios (K_D) for the field samples were generally higher than those observed in the laboratory, averaging $1250\,L\,kg^{-1}$ (Fig. 14 D).

4. Discussion

4.1. The partitioning of barium between the dissolved and adsorbed phases

The measured mass distribution ratios are all greater than unity, indicating that a higher mass of fluid-mobile barium is partitioned into the adsorbed phase compared to the dissolved phase, per unit mass of adsorbent (experiment water density ≈ $1\,kg\,L^{-1}$). The partitioning of barium between the water and the adsorbent surface varied systematically depending on the mineral used, with the order of highest average distribution ratio being: montmorillonite > ferrihydrite > kaolinite > goethite. This order is partly influenced by surface area. Normalising the mean reversible distribution ratio to the surface area of the adsorbent reveals that clay minerals have a higher capacity to adsorb barium per unit area compared to iron oxyhydroxides under the experimental conditions (montmorillonite = $40\,L\,kg^{-1}\,m^{-2}$, kaolinite = $1.8\,L\,kg^{-1}\,m^{-2}$, ferrihydrite = $1.3\,L\,kg^{-1}\,m^{-2}$, goethite = $0.3\,L\,kg^{-1}\,m^{-2}$).

The distribution ratios quantified for kaolinite experiments in this study are similar to batch experiments performed by Eylem et al. (1990); however, the distribution ratios quantified for montmorillonite in the study of Eylem et al. are lower by up to a factor of approximately 25. Multiple differences in the materials used between the two studies complicate the attribution of barium fluid–mobile partitioning differences to specific variables. One significant difference is the greater cation exchange capacity (CEC) of the montmorillonite used in this study compared to Eylem et al. (1990) (this study: SWy–2 = $85\,cmol_c/kg$; Borden and Giese, 2001; Eylem et al., 1990 = 19–$23\,cmol_c/kg$). An increase in the CEC is expected to increase the proportion of barium adsorbed, however, the relationship between the CEC and K_D may be non-linear due to the competition between ions for surface sites. Variations in aqueous chemistry may also factor in. Increased ionic strength typically reduces the partitioning of divalent cations relative to monovalent cations, which aligns with the lower K_D observed for BU100 compared to HS50 in this study (Gaines and Thomas, 1953). The waters used in the experiments of Eylem et al. (1990) had a similar ionic strength to HS50. Eylem et al. also replaced HCO_3^- with NO_3^- to reduce the saturation state of the waters with respect to carbonate minerals. The anionic composition of aqueous fluids is known to impact cation adsorption through changes in aqueous complexation, co-adsorption, and anion exclusion (Sposito et al., 1983; Griffioen and Appelo, 1993). Overall, it is unsurprising that the distribution coefficients vary between the studies given the numerous differences in materials used.

The ability of iron oxyhydroxides to adsorb barium was inversely correlated with the iron-oxyhydroxide-to-water ratio. Barium binding to iron oxyhydroxides has previously been attributed to the formation of tetranuclear complexes with surface hydroxyl groups (Sajih et al., 2014; Sverjensky, 2006). The amphoteric, pH-dependent nature of these hydroxyl bonds result in a dynamic feedback between the chemistry of the mineral surface and the solution. For both goethite and ferrihydrite, barium adsorption is known to increase with the pH of the

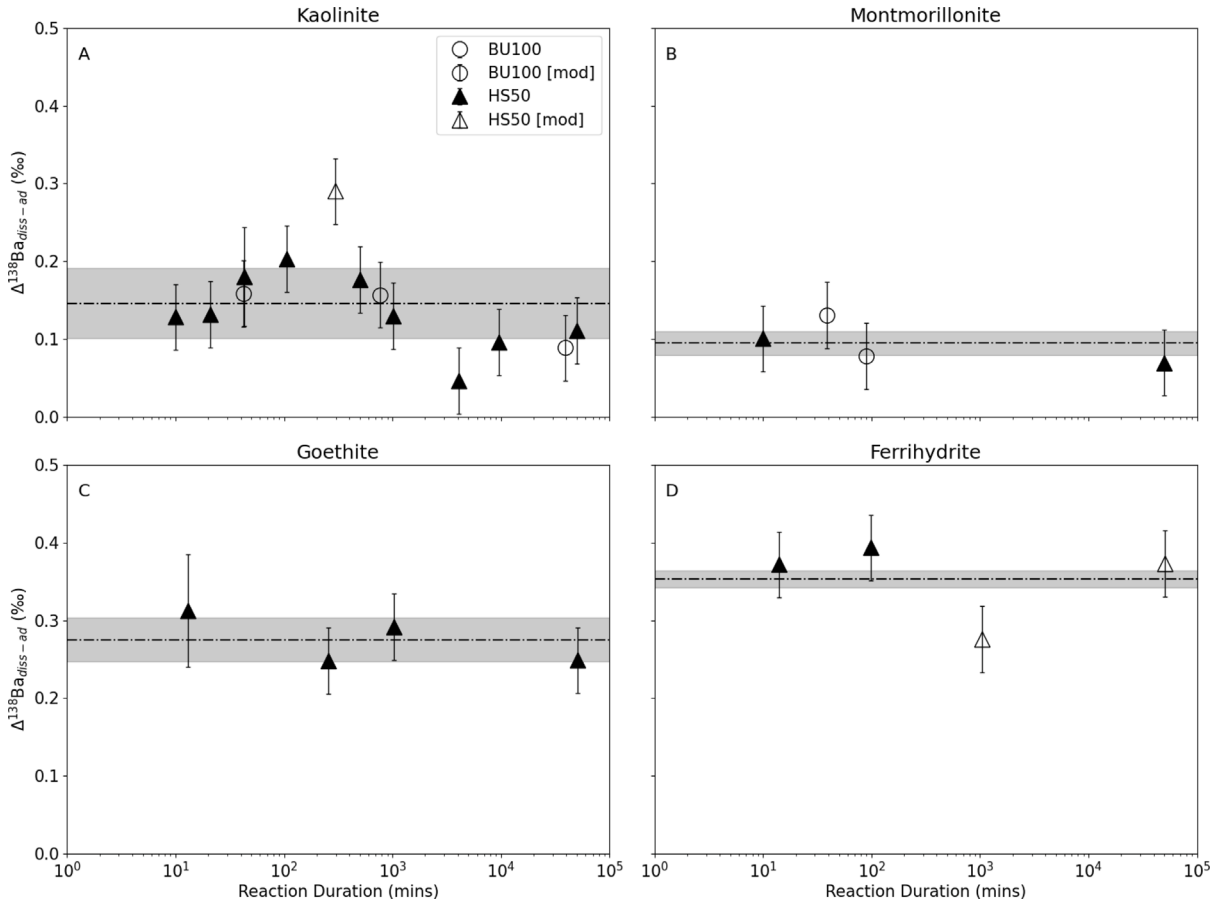

Fig. 9. The offset between the adsorbed and dissolved isotope ratios ($\Delta^{138}Ba_{diss-ad}$) as a function of reaction duration. Error bars represent twice the standard deviation. For measurements without a paired phase, the offset is modelled using the law of mass conservation. White circles indicate experiments performed with BU100, while black triangles represent experiments with HS50. The mean offset is shown by the dot-dashed line, with the grey shaded region representing the standard deviation.

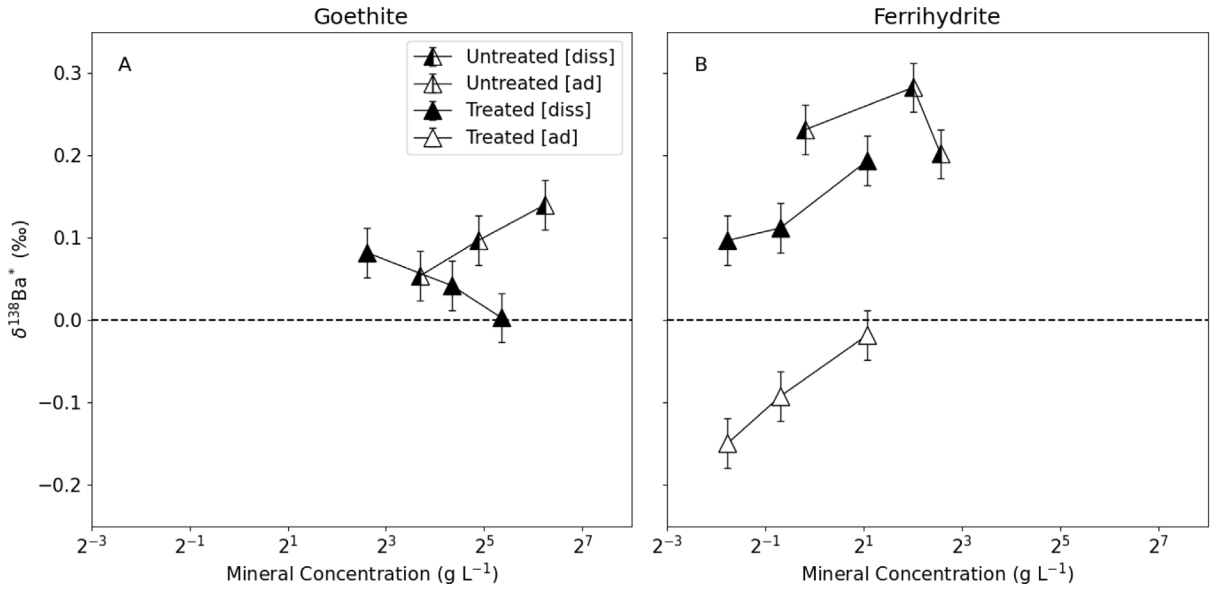

Fig. 10. Barium isotope ratios ($\delta^{138}Ba^{*}$), normalised to the isotopic ratio of the initial experiment water, measured for the leached adsorbed (black) and dissolved (white) phases as a function of the adsorbent concentration. Error bars display twice the standard deviation of repeated standard measurements.

fluid (Sajih et al., 2014). In the experiments, higher iron–oxyhydroxide-to-water ratios would have elevated the ratio of mineral-bound protons to protons in solution, potentially reducing the ability of the iron oxyhydroxides to deprotonate. This reduced deprotonation might explain the lower proportion of barium adsorbed. Clay minerals also possess surface functional groups, however, a significant proportion of their net surface charge arises from permanent structural charge imbalances due to isomorphic lattice substitutions or redox-sensitive elements (Schroth

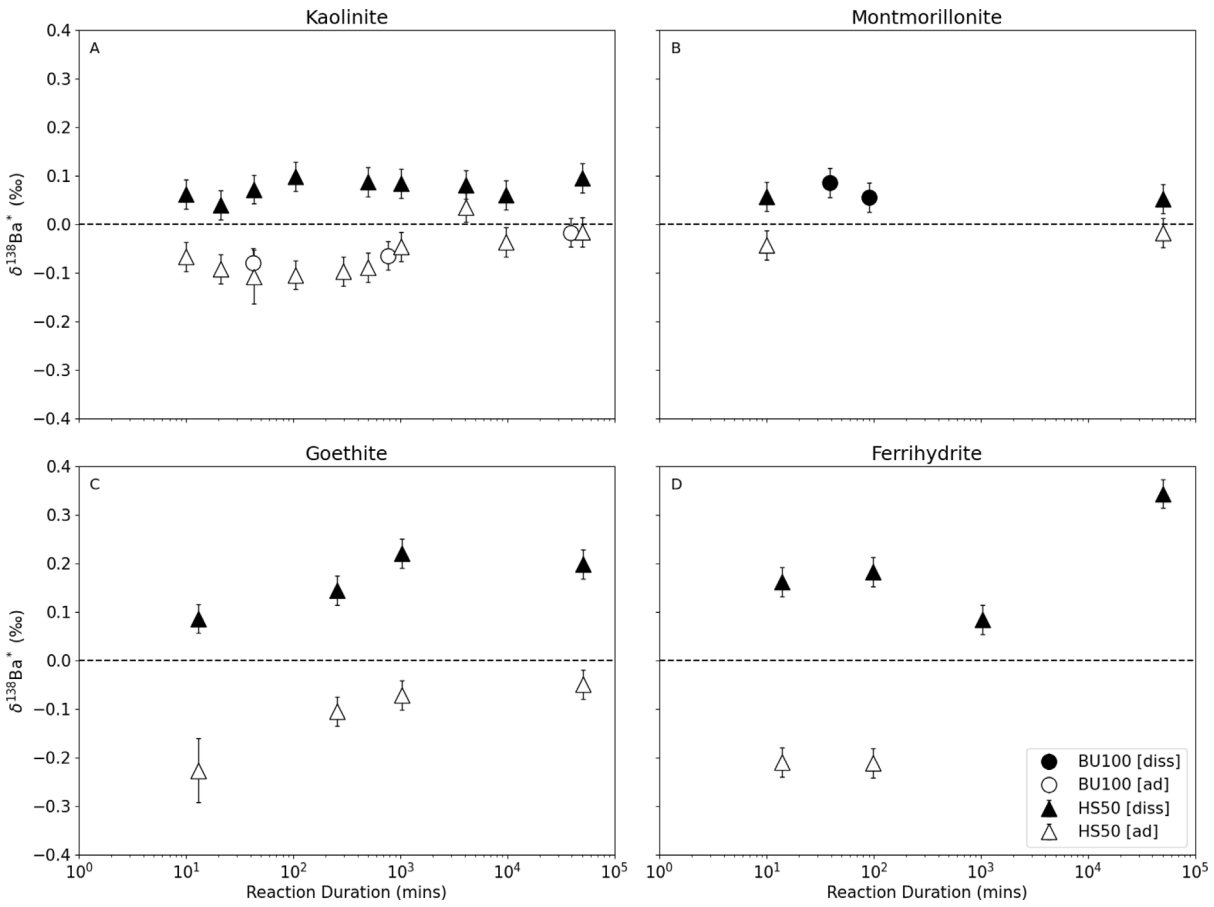

Fig. 11. Barium isotope ratios ($\delta^{138}Ba^*$), normalised to the isotopic ratio of the initial experiment water, measured for the leached adsorbed (black) and dissolved (white) phases as a function of reaction duration. Error bars represent twice the standard deviation of repeated standard measurements.

and Sposito, 1997; Tournassat et al., 2016; Sposito et al., 1999). This difference may account for why this behaviour is observed only in the iron oxyhydroxide experiments.

Although barium is strongly partitioned into the adsorbed phase in the experiments and field samples, the greater affinity of barium for the adsorbed phase of field samples is not replicated in the laboratory experiments (Fig. 14). Field samples often contain significant proportions of minerals with low CECs, such as quartz and feldspar. This suggests that, either there is an adsorbent present in the field samples with a higher selectivity for barium than the minerals studied, or there are significant differences between the conditions of the riverine environment and those in the laboratory experiments. Further investigations into the phase association of adsorbed barium in the field samples could help identify other potential adsorbents, such as organic matter or manganese oxides, that may contribute to the observed differences in selectivity.

4.2. The likelihood of chemical & isotopic steady-state for riverine samples

Chemical and isotopic equilibrium between the adsorbed and dissolved phases is determined by the kinetics of the reactions and the contact time between the phases. To understand the equilibrium state of riverine samples, it is essential to consider the contact times of these phases within the subsurface/regolith and during riverine transport. Fluid transit times within catchments exhibit significant spatial and temporal complexity (Maher, 2011; Floury et al., 2024). For instance, White et al. (2009) used a chloride mass balance technique to estimate regolith pore-fluid residence times, finding them to range between 10 and 24 yr across a regolith chronosequence. The contact time between adsorbed and dissolved phases within rivers is likely to be much shorter, depending largely on sediment transport dynamics.

A wide range of chemical reaction rates have been documented for aqueous adsorption–desorption reactions, with the time to reach chemical equilibrium in experiments varying from seconds (Tang and Sparks, 1993) to days (Li and Liu, 2020). These rates are influenced by several factors: the type of adsorbent, the adsorbate, the chemistry of the solution, and the experimental conditions. In the experiments of this study, the time to achieve chemical steady-state varied primarily as a function of the mineral used. For instance, experiments with montmorillonite and goethite reached chemical steady-state in under 1000 min. Similarly, kaolinite experiments using HS50 also achieved steady-state within approximately 1000 min. In contrast, ferrihydrite experiments initially reached a pseudo-steady-state before experiencing a significant decrease in dissolved barium concentration after around 1000 min. These findings are consistent with the results of Li and Liu (2020), who observed a similar timescale for lithium to reach chemical steady-state using the same adsorbent (KGa-2). Although their experiments were conducted under different conditions — using LiCl solutions of varying ionic strengths, with pH ranging from 3 to 10 and an adsorbent concentration of 10 g L^{-1} — the comparable timescales suggest that the type of adsorbent plays a crucial role in the rate of adsorption–desorption reactions.

Continuous 3 s logging of pH during a replicate montmorillonite experiment provided further insights into the chemistry of the reactions, notably before the shortest reaction duration. In this experiment, the pH initially decreased from 7.9 to 7.7 over approximately 20 s, before gradually rising to 7.8 over 500 min (Fig. S.6). Protons are integral for adsorption–desorption processes, either through the compensation of structural charge imbalances or via bonding to surface functional

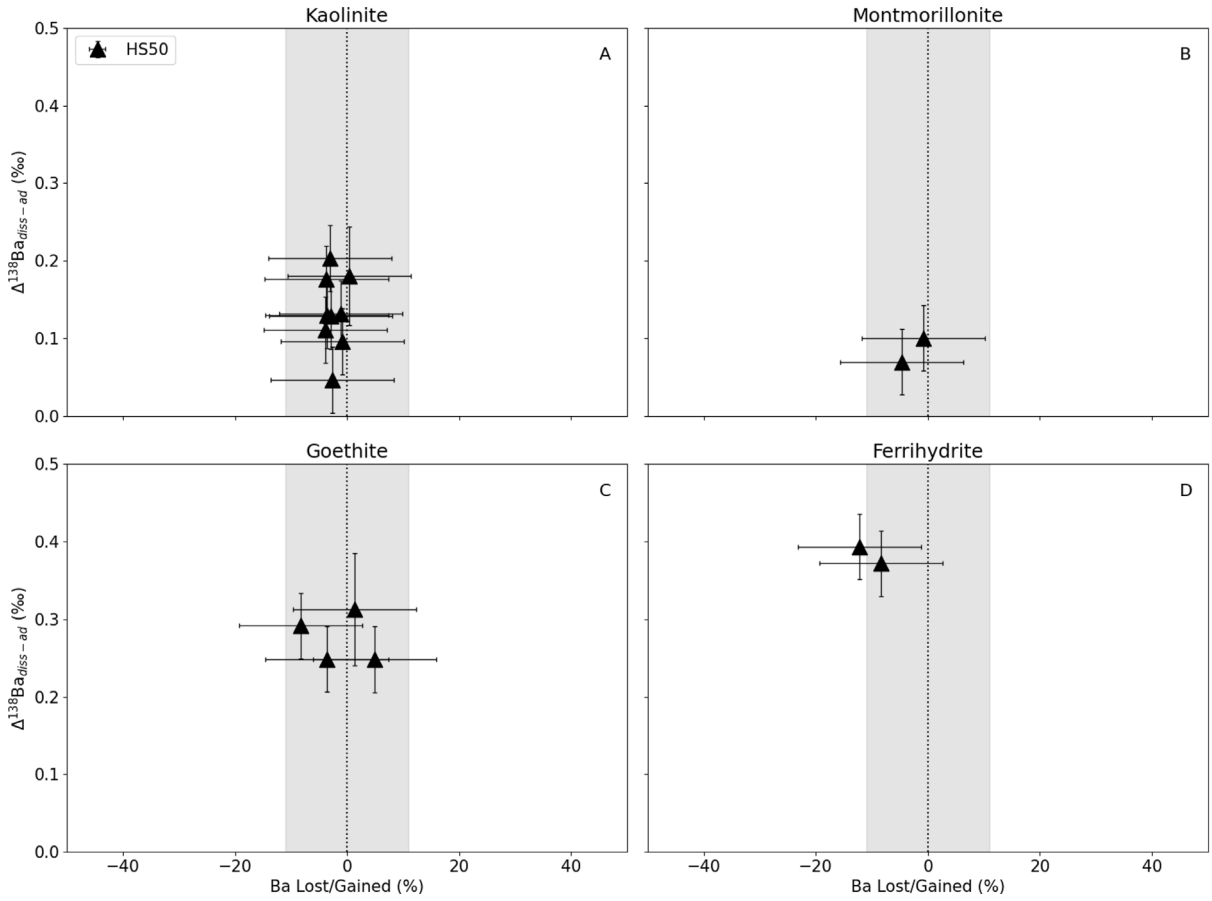

Fig. 12. The offset between the adsorbed and dissolved isotope ratios ($\Delta^{138}Ba_{diss-ad}$) as a function of the barium lost or gained. The loss or gain of barium is calculated relative to the initial barium inventory. Error bars display twice the standard deviation of standard measurements. The mean and standard deviation of the offsets, fitted through both the measured and modelled values, are shown by the dot-dashed line and grey shaded region respectively.

groups. The initial drop in pH can be attributed to the adsorbent's prior exposure to a more acidic reagent (pH of 1.0 M NH_4Cl ~4.6). The subsequent gradual pH increase likely results from the slower re-equilibration of the aqueous carbon system. This re-equilibration could occur through slow CO_2 diffusion from the centrifuge tube's headspace to the laboratory, or through the dissolution of the montmorillonite itself. These temporal pH dynamics underscore the complex and dynamic interplay between adsorption–desorption reactions, mineral dissolution-precipitation processes, and the carbon system. Gaining a deeper understanding of this dynamic coupling would be beneficial for enhancing silicate weathering rates through the application of rock powders to soils, as such interventions aim to perturb the aqueous carbon system which is buffered by the adsorbed phase.

Despite the dynamic coupling between the aqueous carbon system and the adsorbed phase, the timescale required to reach chemical steady-state in most of the experiments conducted in this study is shorter than the pore-fluid regolith residence times previously observed. This aligns with the chemical equilibrium observed between pore-fluids and the adsorbed phase in regolith profile studies (White et al., 2009). Although several factors in river systems could hinder the attainment of true chemical equilibrium — such as fluctuating sediment and water inputs, hydrodynamic sorting, competitive inhibition by other cations, and the degassing and ingassing of carbon dioxide — radiogenic strontium isotope measurements of the adsorbed and dissolved phases in rivers are typically within analytical uncertainty of each other (Tipper et al., 2020). This suggests that the adsorption–desorption reaction rates for strontium in rivers are sufficiently rapid to prevent detectable differences between these phases, providing promising evidence that adsorbed and dissolved barium isotopes in river systems might also be at or near chemical equilibrium.

The identification of isotopic steady-state in the experiments is more challenging than detecting chemical steady-state due to the lower temporal resolution of the isotopic measurements (Fig. 11). It has previously been observed that chemical equilibrium is reached before isotopic equilibrium (Zeebe et al., 1999; Pearce et al., 2012). The time to achieve chemical equilibrium therefore provides a lower bound on the timescale needed to achieve isotopic equilibrium. In the experiments conducted, only kaolinite and goethite appear to have reached isotopic steady-state, occurring after approximately 1000 min and 250 min, respectively. This timeframe is similar to that over which chemical steady-state was obtained.

4.3. Isotope fractionation mechanisms and mass-balance frameworks

Stable isotope fractionation reactions can be modelled as equilibrium or kinetic processes in closed or open systems. The type of process and system impacts the magnitude of the isotopic fractionation and can have implications for the mass-balance frameworks used to interpret Critical Zone processes. For closed-system equilibrium isotope fractionation to occur, the adsorption–desorption reactions must operate in a well-mixed system. Open-system isotope fractionation can be modelled by Rayleigh fractionation, provided the isotopic species removed at every instant were in thermodynamic and isotopic equilibrium with those remaining in the system. Closed-system equilibrium isotope fractionation therefore requires a high degree of reaction reversibility between the phases, whereas Rayleigh isotope fractionation requires part isolation of a phase.

Batch and Rayleigh models were fitted to the data as a function of the fraction of barium adsorbed (Fig. 15). These models were applied

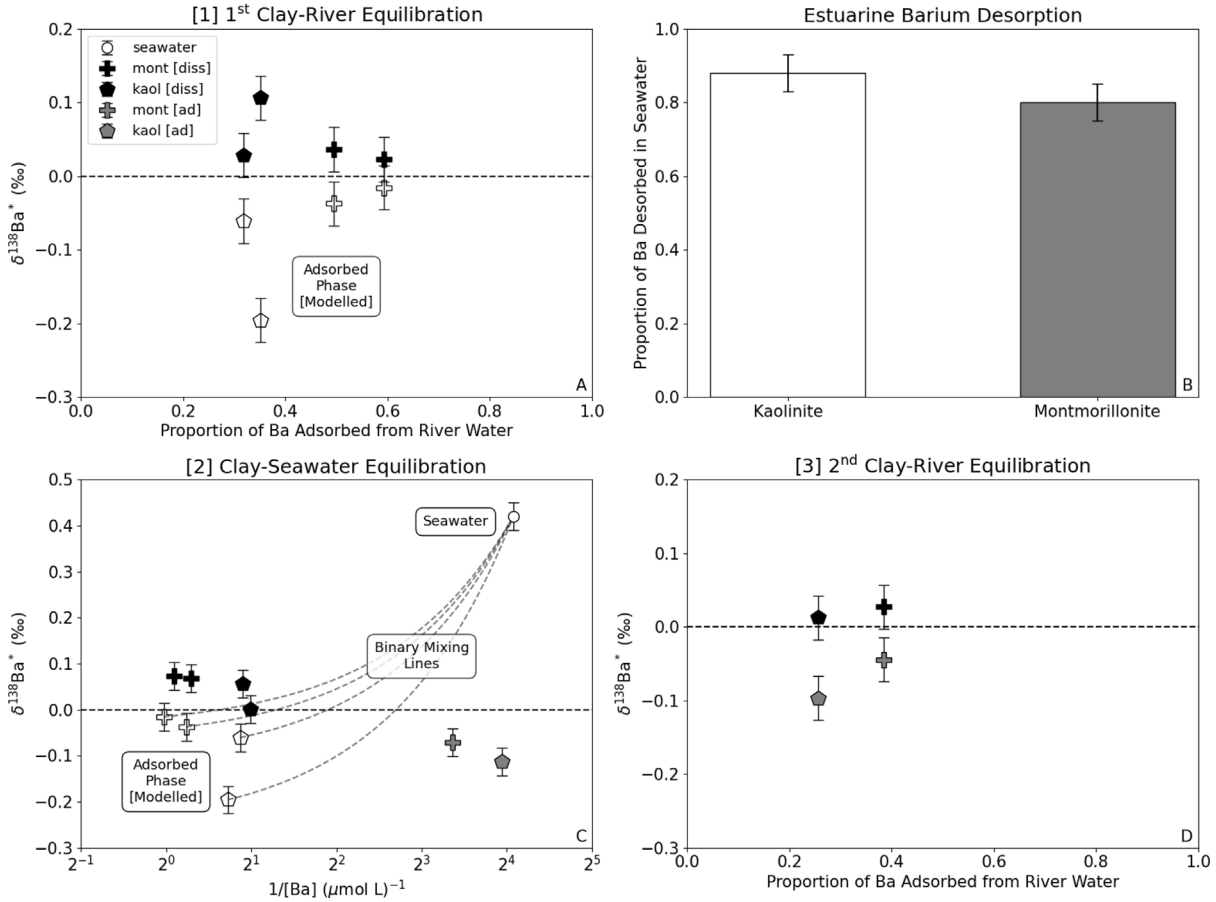

Fig. 13. Measured and modelled barium isotope ratios during the estuarine adsorption–desorption experiments. A: The dissolved (measured) and adsorbed (modelled) barium isotope ratios following the addition of river water (HS50) to clay minerals (kaolinite and montmorillonite). B: The proportion of barium desorbed from river–water-equilibrated clay minerals following the addition of seawater. C: The measured adsorbed and dissolved barium isotope ratios during mixing of river-water-equilibrated clay minerals and seawater (SWH). The mixing lines connect seawater to the modelled adsorbed values from the first river water equilibration step. D: The measured adsorbed and dissolved barium isotope ratios following the second addition of river water to seawater-equilibrated clay minerals.

Table 1
The mean fractionation factors ($\alpha_{ad-diss}$), standard deviation (σ), and sample count (N) for each mineral using two standard isotope fractionation models: closed-system equilibrium (CSE) and Rayleigh.

Method	Parameter	Kaolinite	Montmorillonite	Goethite	Ferrihydrite
CSE	$1-\alpha$	1.2×10^{-4}	8.0×10^{-5}	2.6×10^{-4}	2.5×10^{-4}
	σ	5.0×10^{-5}	4.0×10^{-5}	1.2×10^{-4}	1.1×10^{-4}
	N	21	6	14	15
Rayleigh	$1-\alpha$	5.0×10^{-5}	5.0×10^{-5}	3.1×10^{-4}	2.3×10^{-4}
	σ	3.0×10^{-5}	3.0×10^{-5}	1.1×10^{-4}	7.0×10^{-5}
	N	21	6	14	15

to the minerals separately, as the magnitude of fractionation was found to have a first-order dependence on the type of adsorbent (Fig. 14). Isotopic fractionation factors were calculated for each model (Section 2.3.7). Neither model was found to represent the data significantly better than the other (S.12.2); however, the dissolved phase is better represented than the adsorbed phase for all minerals.

Differences in the average magnitude of barium isotope fractionation were observed across various minerals (Table 1), which may be linked to variations in the strength of bonding between barium and the mineral surfaces. The net surface charge of clay minerals, like montmorillonite and kaolinite, derive from a mixture of surface functional groups and permanent charge sites (Tournassat et al., 2016; Faivre, 2016). The surface charge of iron oxyhydroxides, on the other hand, primarily derives from hydroxyls. Adsorption to permanent surface charge sites on clay minerals is typically achieved by outer-sphere bonding, while inner-sphere coordination bonds are more common at surface functional group sites (Zhang et al., 2001; Li and Liu, 2020). The stronger inner-sphere bonding observed for iron oxyhydroxides could account for the greater degree of barium isotope fractionation observed with these minerals, reflecting a more substantial effect on the fractionation process.

The degree of reversibility of barium adsorption varied consistently among different minerals (Fig. 7). Complete recovery of barium was observed in experiments with kaolinite and goethite, suggesting that closed-system equilibrium fractionation might be a suitable model for these minerals. Montmorillonite experiments exhibited lower recovery rates, and ferrihydrite experiments initially showed about 85% recovery; however, this decreased over time, with lower recovery observed after 1000 min. No correlation was observed between the degree of reversibility and the duration of the experiment, the chemistry of the water, or with the expected type of bonding.

The transformation of ferrihydrite to more stable iron oxyhydroxides has previously been shown to trap adsorbed metals (Lu et al., 2020), and could provide a process by which barium is irreversibly adsorbed. Batch experiments performed by Sajih et al. (2014), using 2-line-ferrihydrite samples synthesised via the same method, observed the transformation of ferrihydrite to geothite; however, no transformation of ferrihydrite to goethite was observed in this study (Fig. S.3). Furthermore, no trapping of barium was identified by Sajih et al. (2014). The lack of observed transformation may result from differences in the XRD anodes used in the studies, with the molybdenum anode used in this study making it more challenging to identify the transformation

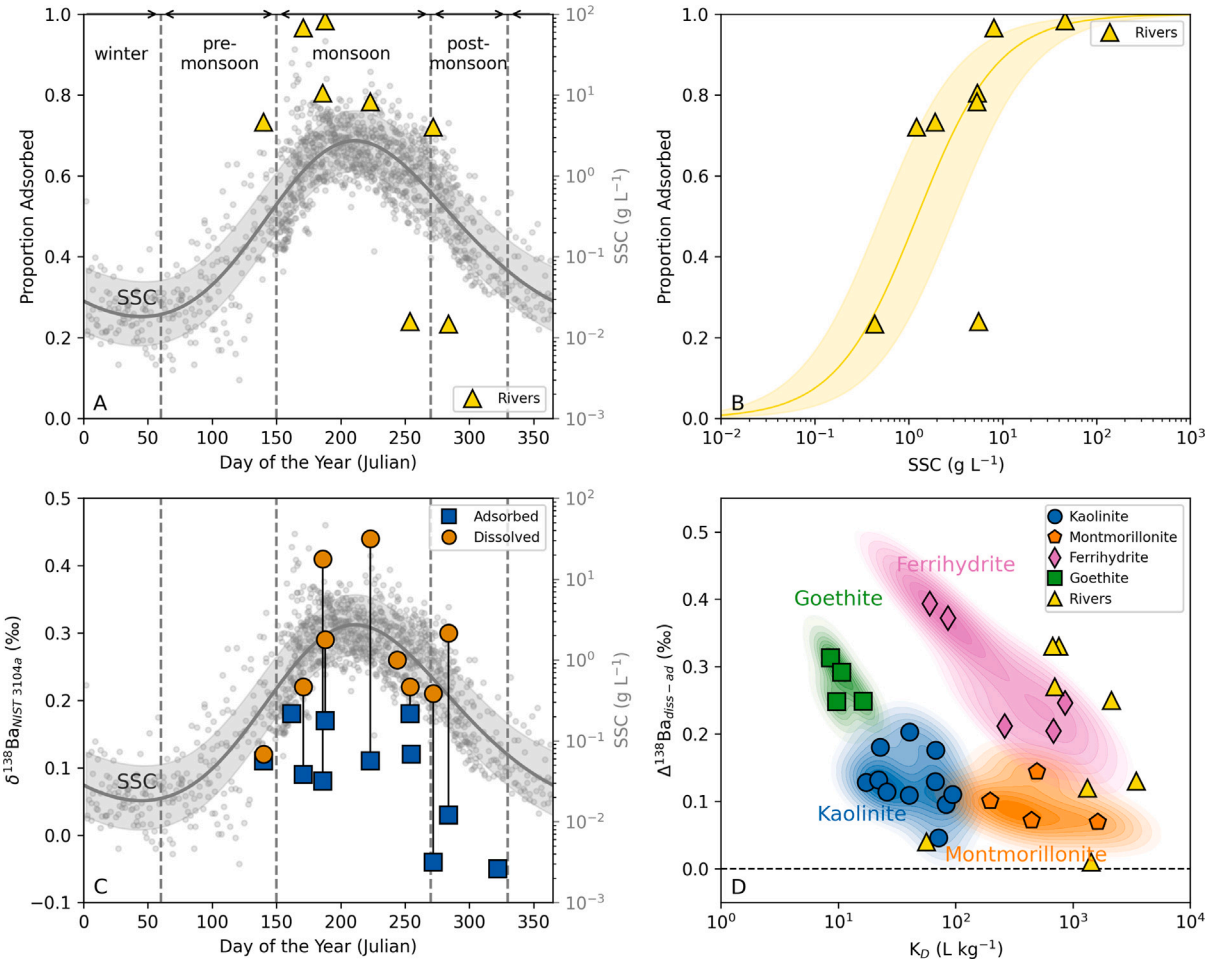

Fig. 14. Adsorbed and dissolved barium proportions and isotope ratios of Himalayan rivers (Saptakoshi and Sunkoshi). A: the proportion of fluid–mobile barium present in the adsorbed phase as a function of the sample collection day. Suspended sediment concentrations (SSC) of the rivers are also plotted (grey markers). B: the proportion of fluid–mobile barium adsorbed as a function of the SSC. C: stable barium isotope ratios of the fluid–mobile phases as a function of the Julian day of the year. D: the $\Delta^{138}Ba_{diss-ad}$ of paired experiment samples from the Riverine Series and field samples, as a function of the reversible distribution ratio (K_D [r]). A bivariate kernel density estimate has been fitted to the mineral data using Scott's bandwidth rule. SSC measurements are from Andermann et al. (2024).

of goethite to ferrihydrite, as the broad [2-line] peaks of ferrihydrite obscure the expected transformation 2θ, compared to the copper anode used by Sajih et al. (2014).

Barite precipitation provides an alternative mechanism for the reduced recovery of adsorbed barium, which can occur even in undersaturated marine fluids potentially driven by interactions with organic matter (Deng et al., 2019; Horner et al., 2017; Martinez-Ruiz et al., 2019). Isotope ratio offsets between barite and dissolved barium observed in laboratory experiments at chemical equilibrium are identical in direction and similar in magnitude with those found in this study ($\Delta^{138}Ba_{barite-dBa} \approx 0.10‰$ (Middleton et al., 2023b); Fig. 15). However, given the low likelihood of significant organic matter concentrations in the experiments of this study, combined with barium recovery degrees that correlate with the mineral used rather than the barite saturation state of the water, barite precipitation is not considered a likely mechanism. The findings of this study suggest that the adsorption of dissolved barium to barite surfaces may provide an additional mechanism for the fractionation of barium in barite-fluid systems. Given that calcium and strontium have both been shown to adsorb to barite surfaces (Bracco et al., 2019; Hang et al., 2007), it is likely that barium will behave similarly.

Montmorillonite inter-layer compaction provides a third process for the irreversible loss of barium. Compaction is known to be strongly coupled to the ion-exchange process (Laird and Shang, 1997; Teich-McGoldrick et al., 2015). The replacement of freshwater with 1 M NH_4Cl or seawater may have resulted in the compaction-induced trapping of barium between basal montmorillonite planes. Irrespective of the driver, closed-system equilibrium fractionation is not an appropriate model for experiments with significant irreversible adsorption of barium.

4.4. A laboratory-field sample comparison and implications for using barium isotope ratios as tracers of weathering and erosion

The offset between the adsorbed and dissolved barium isotope ratios of field samples is consistent in magnitude and direction with the experiments (Fig. 16), whereas the only other laboratory investigation to determine the fractionation of barium isotopes during adsorption–desorption reactions discovered an opposite direction of fractionation (van Zuilen et al., 2016). van Zuilen et al. used varying concentrations of $BaCl_2$ (0.1 M and 1.0 M) and silica hydrogel as the adsorbent, suggesting that either amorphous silica is not a significant component in the natural samples measured or that the conditions in the experiments do not fully capture the adsorption–desorption processes in rivers.

The fractionation direction observed in this study aligns with a number of other laboratory studies on adsorption–desorption reactions involving alkali and alkali-earth metals and clay minerals (calcium: kaolinite, montmorillonite, and muscovite Brazier et al., 2019; lithium: kaolinite Li and Liu, 2020; strontium: montmorillonite Liu et al., 2022). The observed fractionation suggests that barium isotopes released from

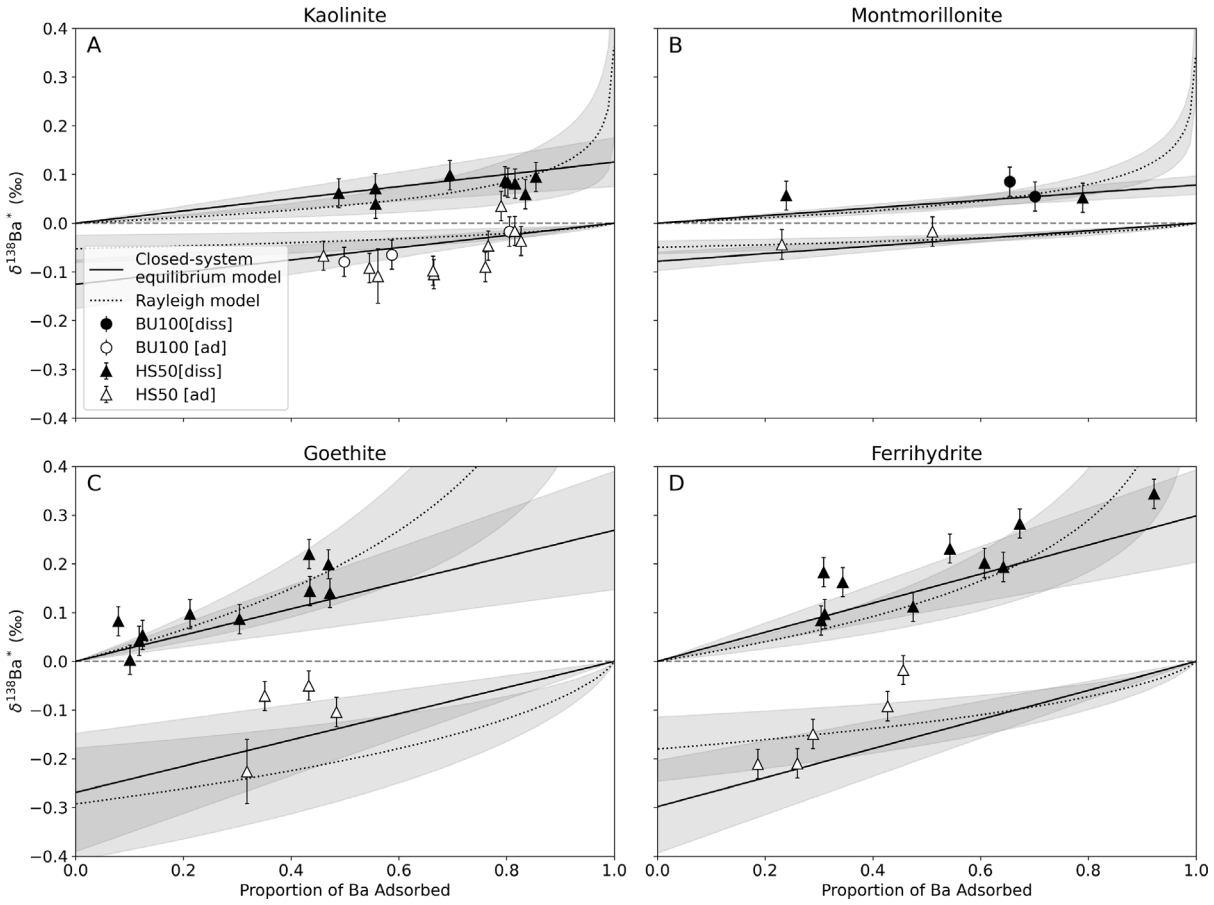

Fig. 15. Stable barium isotope ratios ($\delta^{138}Ba^*$), expressed relative to the isotope ratio of the initial experimental water, as a function of the fraction of total barium adsorbed. Marker face colours denote the phase: white (adsorbed) and black (dissolved). Closed-system equilibrium and Rayleigh isotopic fractionation models were fitted to the data using a square-residual misfit technique. The grey shaded regions represent the standard deviation of the model.

bedrock dissolution preferentially partition into a lighter adsorbed reservoir and a heavier dissolved reservoir. This could explain the heavy isotope enrichment of the dissolved phase in rivers relative to bedrock (Gou et al., 2020). Additionally, the adsorbed reservoir typically contains orders of magnitude more barium than the biological reservoir, which has been previously suggested as the complementary phase responsible for this enrichment (Charbonnier et al., 2020). Increasing field observations for both reservoirs would provide a clearer understanding of the relative contributions of these processes to the observed isotope enrichment (Fig. 1).

Both lithium and barium originate from the weathering of silicate minerals, but the greater partitioning of barium into the adsorbed phase compared to lithium suggests that riverine isotope ratios of these elements may respond differently to weathering processes (Dalai et al., 2002; von Strandmann et al., 2020). Barium, with a more negative hydration enthalpy than lithium, tends to be more readily adsorbed to sediment surfaces (Teppen and Miller, 2006; Knight et al., 2024). In contrast, lithium isotopes (δ^7Li) are strongly fractionated during the formation of secondary weathering products, making them useful for tracing the intensity of silicate weathering (Dellinger et al., 2015; Hindshaw et al., 2019; Li and Liu, 2020; Misra and Froelich, 2012).

The differing kinetics of precipitation–dissolution and adsorption–desorption reactions are likely to impact the utility of alkali and alkaline-earth stable isotope systems, despite the two reactions often being interlinked. Clay mineral precipitation–dissolution reactions are commonly slower compared to adsorption–desorption reactions under earth-surface conditions, limiting the likelihood of achieving chemical and isotopic equilibrium between clay minerals and fluids (Yang and Steefel, 2008). Consequently, clay-bound and dissolved lithium isotopes are likely to be at a state of disequilibrium in systems where the contact time between phases is shorter (lower Damköhler numbers). Given that a larger proportion of barium is partitioned into the adsorbed phase compared to lithium, and considering the faster reaction rates between fluid–mobile phases, barium isotope ratios are more likely to be at chemical and isotopic equilibrium. This particular behaviour lends itself to tracing more rapid weathering zone processes, such as perturbations to terrestrial soil nutrient stocks. Comparative studies of lithium and barium stable isotopes in catchments with varying weathering intensities would help to truth if the differences in adsorption affinity influence the isotopic behaviour.

Barium isotope ratios have demonstrated potential as high–resolution (monthly) tracers of riverine inputs to the ocean, as evidenced by measurements of marine paleo-archive samples such as corals (Yu et al., 2022). This proxy depends on understanding barium desorption from freshwater-derived suspended sediment in estuaries. Bridgestock et al. (2021) estimated that between 20 and 75% of the dissolved riverine input to the oceans is sourced from estuarine processes. The estuarine experiments in this study confirm that the majority of barium (77% to 94%) is desorbed during the mixing of fresh and saline waters, indicating paleo-archives of barium situated near significant riverine and groundwater inputs to the ocean are therefore likely to reflect both adsorbed and dissolved riverine inputs.

Distinct differences in concentration and isotopic composition of stable barium isotopes between fresh and saline waters, coupled with measurable fractionation during adsorption–desorption reactions, provide promising evidence that stable barium isotope ratios could also be used to trace other freshwater-saline interactions, such as the buffering of aquifers by the adsorbed phase. The salinisation of aquifers is an

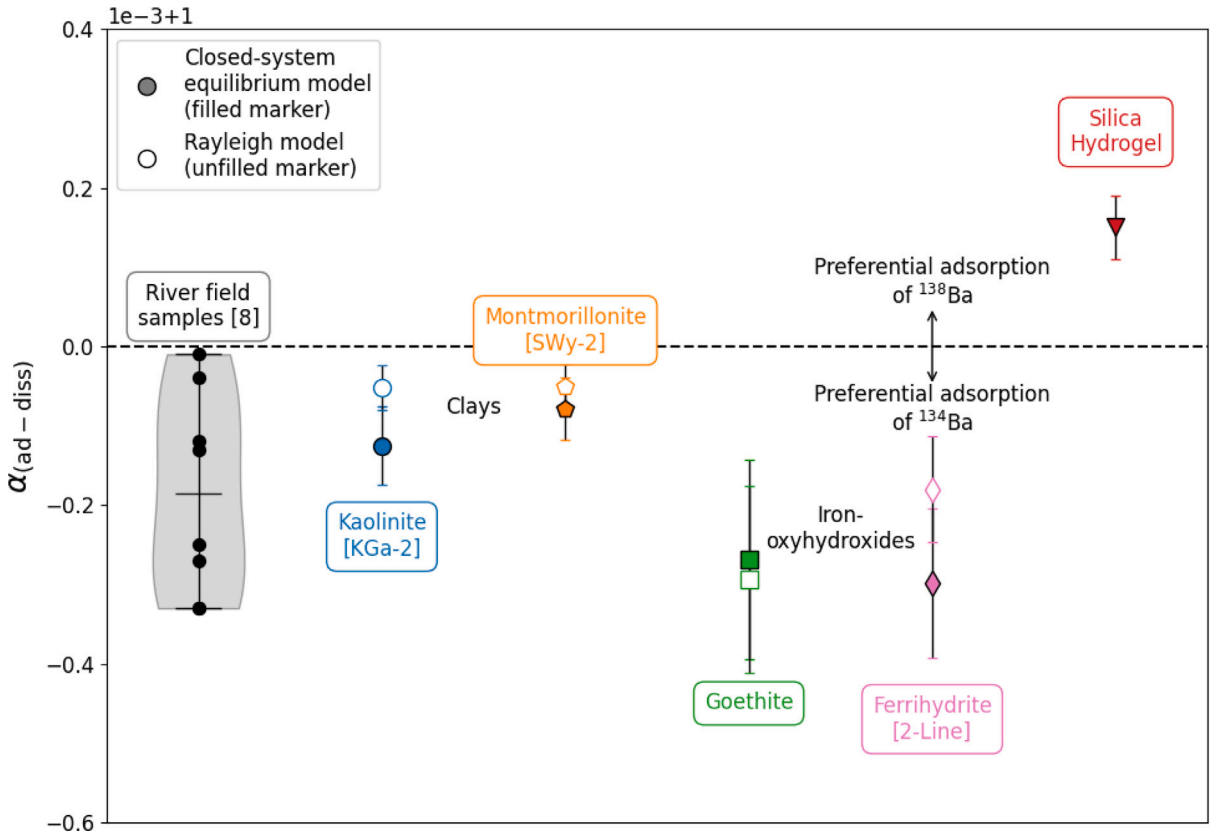

Fig. 16. A comparison of between α measurements of riverine field samples and laboratory experiments (Table 1). The fractionation during adsorption to silica hydrogel is also shown (van Zuilen et al., 2016). Riverine field samples are plotted as a violin plot, with the mean shown. Error bars display the standard deviation.

escalating global issue driven by the dual stresses of increasing freshwater demand and climate change (Kaushal et al., 2021). Overall, the results of this study offer the required constraints on the magnitude and direction of barium isotope fractionation to enable more extensive modelling efforts, opening up new avenues for using barium isotope ratios as tracers of environmental processes.

5. Conclusions

This study provides significant insights into the behaviour of barium isotopes during adsorption–desorption reactions in both controlled laboratory experiments and natural riverine environments. Adsorption–desorption reactions were found to enrich the adsorbed phase in the lighter barium isotope (^{134}Ba) and the water in the heavier barium isotope (^{138}Ba). The magnitude of isotopic fractionation was found to vary primarily based on the type of mineral adsorbent, with clays generally exhibiting less fractionation than iron oxyhydroxides. The magnitude and direction of the isotopic fractionation was sufficient to explain the natural variability measured in the Himalayan river samples. The reactions were also found to be rapid relative to the transit time of sediment and water in continental catchments, and largely reversible. The extent of reversibility, however, depended on the specific mineral involved. Complete recovery of barium was achieved for the kaolinite and goethite experiments through repeated additions of 1 M NH_4Cl, while recovery from montmorillonite varied between 59% and complete recovery. A significant decrease in the recovery of barium from ferrihydrite was observed after a duration of 1000 min. Estuarine experiments, designed to replicate sediment passage through a salinity gradient, showed a high degree of reversibility, with 77% to 94% of the adsorbed barium being desorbed upon the addition of seawater to freshwater-equilibrated clay minerals. Consequently, barium isotope ratios measured in marine paleo-archives are expected to reflect both the adsorbed and dissolved freshwater barium inputs to the ocean. The high-temporal resolution monitoring of pH during the experiments underscored the dynamic coupling between adsorption–desorption reactions and the aqueous carbon system. The findings suggest that due to rapid reaction rates, a high degree of reaction reversibility, and the strong affinity of barium for the adsorbed phase, riverine barium isotope ratios may offer unique insights into weathering and erosion processes compared to more widely used alkali and alkaline-earth stable isotope ratios (e.g., δ^7Li, δ^{44}Ca).

CRediT authorship contribution statement

Alasdair C.G. Knight: Writing – review & editing, Writing – original draft, Visualization, Validation, Methodology, Investigation, Formal analysis, Data curation, Conceptualization. **Edward T. Tipper:** Writing – review & editing, Resources, Funding acquisition, Conceptualization. **Harold J. Bradbury:** Writing – review & editing, Resources. **Alexandra V. Turchyn:** Writing – review & editing, Resources. **Christoff Andermann:** Writing – review & editing, Resources. **Heye Freymuth:** Writing – review & editing, Resources. **Tim Elliott:** Writing – review & editing, Resources. **Luke Bridgestock:** Writing – review & editing, Validation, Methodology, Conceptualization.

Declaration of competing interest

The authors declare that they have no known competing financial interests or personal relationships that could have appeared to influence the work reported in this paper.

Data availability

Barium concentrations and isotope ratios are available through NERC EDS Environmental Information Data Centre at https://doi.org/10.5285/cfa9abd4-1200-47b6-9553-aa1b6e4d9ffd. Powder XRD measurements are available through Zenodo at https://doi.org/10.5281/zenodo.13257704.

Acknowledgements

Dr. Julien T. Middleton, Dr. Tarun K. Dalai, and an anonymous reviewer are all thanked for their helpful reviews and thoughtful comments, which significantly improved the manuscript. Dr. Tristan J. Horner is also acknowledged as the editor for his critical suggestions to enhance the manuscript. Alasdair Knight was funded by a NERC DTP studentship (NE/S007164/1). This research was supported by a Leverhulme Trust Early Career Fellowship (ECF-2019-049), backed by the Isaac Newton Trust, awarded to Luke Bridgestock, as well as a NERC grant awarded to Edward Tipper (NE/T007214/1). Special thanks go to Dr. Marie-Laure Bagard for her continual assistance in the isotope clean laboratories at the Department of Earth Sciences, University of Cambridge. Dr. Rosa M. Danisi is also thanked for guidance with the XRD at the Department of Earth Sciences, University of Cambridge.

Appendix A. Supplementary data

The following sections are available in the supplementary information file: S.1: Purification of Montmorillonite via Settling (SWy–2); S.2: Laboratory Synthesis of Iron Oxyhydroxides; S.3: Powder X-ray Diffraction (XRD); S.4: Surface Area Analysis; S.5: Scanning Electron Microscope (SEM) Images; S.6: The Dissolved Chemistry of Experiment Waters & Mineral Saturation Indicies; S.7: Using High Temporal Frequency pH Measurements to Track Adsorption-Desorption Reactions; S.8: Optimising the Desorption Method; S.9: Quantifying the Dissolved and Adsorbed Element Concentrations; S.10: Details of the Analytical Methods for Barium Isotope Measurements; S.11 Reaction Kinetics; S.12 Isotopic Fractionation Models.

Supplementary material related to this article can be found online at https://doi.org/10.1016/j.gca.2024.08.016.

References

Andermann, C., Crave, A., Gloaguen, R., Davy, P., Bonnet, S., 2012. Connecting source and transport: Suspended sediments in the Nepal Himalayas. Earth Planet. Sci. Lett. 351–352, 158–170.

Andermann, C., Puhl, D., Zimmermann, B., Hughes, G., Sitaula, A.P., Adhikari, B.R., Baidya, K.P., 2024. PRESSurE suspended sediment data time series, Gorkha earthquake, Nepal. http://dx.doi.org/10.5880/GFZ.4.6.2023.001.

Bates, S.L., Hendry, K.R., Pryer, H.V., Kinsley, C.W., Pyle, K.M., Woodward, E.M.S., Horner, T.J., 2017. Barium isotopes reveal role of ocean circulation on barium cycling in the Atlantic. Geochim. Cosmochim. Acta 204, 286–299.

Borden, D., Giese, R.F., 2001. Baseline studies of the clay minerals society source clays: Cation exchange capacity measurements by the ammonia-electrode method. Clays Clay Miner. 49 (5), 444–445.

Bracco, J.N., Lee, S.S., Stubbs, J.E., Eng, P.J., Jindra, S., Warren, D.M., Kommu, A., Fenter, P., Kubicki, J.D., Stack, A.G., 2019. Simultaneous adsorption and incorporation of strontium(II) at the barite (001)-water interface. J. Phys. Chem. C 123 (2), 1194–1207, Publisher: American Chemical Society.

Brantley, S.L., Goldhaber, M.B., Ragnarsdottir, K.V., 2007. Crossing disciplines and scales to understand the critical zone. Elements 3 (5), 307–314.

Brazier, J.-M., Schmitt, A.-D., Gangloff, S., Pelt, E., Chabaux, F., Tertre, E., 2019. Calcium isotopic fractionation during adsorption onto and desorption from soil phyllosilicates (kaolinite, montmorillonite and muscovite). Geochim. Cosmochim. Acta 250, 324–347.

Bridgestock, L., Hsieh, Y.-T., Porcelli, D., Homoky, W.B., Bryan, A., Henderson, G.M., 2018. Controls on the barium isotope compositions of marine sediments. Earth Planet. Sci. Lett. 481, 101–110.

Bridgestock, L., Nathan, J., Paver, R., Hsieh, Y.-T., Porcelli, D., Tanzil, J., Holdship, P., Carrasco, G., Annammala, K.V., Swarzenski, P.W., Henderson, G.M., 2021. Estuarine processes modify the isotope composition of dissolved riverine barium fluxes to the ocean. Chem. Geol. 120340.

Bullen, T., Chadwick, O., 2016. Ca, Sr and Ba stable isotopes reveal the fate of soil nutrients along a tropical climosequence in Hawaii. Chem. Geol. 422, 25–45.

Cao, Z., Siebert, C., Hathorne, E.C., Dai, M., Frank, M., 2020. Corrigendum to "Constraining the oceanic barium cycle with stable barium isotopes" [Earth Planet. Sci. Lett. 434 (2016) 1–9]. Earth Planet. Sci. Lett. 530, 116003.

Charbonnier, Q., Bouchez, J., Gaillardet, J., Calmels, D., Dellinger, M., 2022. The influence of black shale weathering on riverine barium isotopes. Chem. Geol. 594, 120741.

Charbonnier, Q., Bouchez, J., Gaillardet, J., Gayer, E., 2020. Barium stable isotopes as a fingerprint of biological cycling in the Amazon River basin. Biogeosciences 17 (23), 5989–6015.

Coffey, M., Dehairs, F., Collette, O., Luther, G., Church, T., Jickells, T., 1997. The behaviour of dissolved barium in estuaries. Estuar. Coast. Shelf Sci. 45 (1), 113–121.

Crockford, P.W., Wing, B.A., Paytan, A., Hodgskiss, M.S.W., Mayfield, K.K., Hayles, J.A., Middleton, J.E., Ahm, A.-S.C., Johnston, D.T., Caxito, F., Uhlein, G., Halverson, G.P., Eickmann, B., Torres, M., Horner, T.J., 2019. Barium-isotopic constraints on the origin of post-Marinoan barites. Earth Planet. Sci. Lett. 519, 234–244.

Dalai, T.K., Krishnaswami, S., Sarin, M.M., 2002. Barium in the Yamuna River System in the Himalaya: Sources, fluxes, and its behavior during weathering and transport. Geochem. Geophys. Geosyst. 3 (12), 1–23.

Dellinger, M., Gaillardet, J., Bouchez, J., Calmels, D., Louvat, P., Dosseto, A., Gorge, C., Alanoca, L., Maurice, L., 2015. Riverine Li isotope fractionation in the Amazon River basin controlled by the weathering regimes. Geochim. Cosmochim. Acta 164, 71–93.

Deng, G., Kang, J., Nan, X., Li, Y., Guo, J., Ding, X., Huang, F., 2021. Barium isotope evidence for crystal-melt separation in granitic magma reservoirs. Geochim. Cosmochim. Acta 292, 115–129.

Deng, N., Stack, A.G., Weber, J., Cao, B., De Yoreo, J.J., Hu, Y., 2019. Organic–mineral interfacial chemistry drives heterogeneous nucleation of Sr-rich (Bax, Sr1-x)SO4 from undersaturated solution. Proc. Natl. Acad. Sci. 116 (27), 13221–13226, Publisher: Proceedings of the National Academy of Sciences.

Eylem, C., Erten, H.N., Göktürk, H., 1990. Sorption-desorption behaviour of barium on clays. J. Environ. Radioact. 11 (2), 183–200.

Faivre, D., 2016. Iron oxides: from nature to applications. John Wiley & Sons.

Floury, P., Bouchez, J., Druhan, J.L., Gaillardet, J., Blanchouin, A., Gayer, E., Ansart, P., 2024. Linking dynamic water storage and subsurface geochemical structure using high-frequency concentration-discharge records. Water Resour. Res. 60 (1).

Foster, D.A., Staubwasser, M., Henderson, G.M., 2004. 226Ra and Ba concentrations in the Ross Sea measured with multicollector ICP mass spectrometry. Mar. Chem. 87 (1), 59–71.

Gaillardet, J., Viers, J., Dupré, B., 2003. 5.09 - Trace elements in river waters. In: Holland, H.D., Turekian, K.K. (Eds.), Treatise on Geochemistry. Pergamon, Oxford, pp. 225–272.

Gaines, Jr., G.L., Thomas, H.C., 1953. Adsorption studies on clay minerals. II. a formulation of the thermodynamics of exchange adsorption. J. Chem. Phys. 21 (4), 714–718.

Gong, Y., Zeng, Z., Cheng, W., Lu, Y., Zhang, L., Yu, H., Huang, F., 2020. Barium isotopic fractionation during strong weathering of basalt in a tropical climate. Environ. Int. 143, 105896.

Gou, L.-F., Jin, Z., Galy, A., Gong, Y.-Z., Nan, X.-Y., Jin, C., Wang, X.-D., Bouchez, J., Cai, H.-M., Chen, J.-B., Yu, H.-M., Huang, F., 2020. Seasonal riverine barium isotopic variation in the middle Yellow River: Sources and fractionation. Earth Planet. Sci. Lett. 531, 115990.

Griffioen, J., Appelo, C.a.J., 1993. Adsorption of calcium and its complexes by two sediments in calcium-hydrogen-chlorine-carbon dioxide systems. Soil Sci. Soc. Am. J. 57 (3), 716–722.

Hang, J.Z., Zhang, Y.F., Shi, L.Y., Feng, X., 2007. Electrokinetic properties of barite nanoparticles suspensions in different electrolyte media. J. Mater. Sci. 42 (23), 9611–9616.

Hartmann, J., Lauerwald, R., Moosdorf, N., 2019. GLORICH - Global river chemistry database. PANGAEA, Type: data set.

Hindshaw, R.S., Tosca, R., Goût, T.L., Farnan, I., Tosca, N.J., Tipper, E.T., 2019. Experimental constraints on Li isotope fractionation during clay formation. Geochim. Cosmochim. Acta 250, 219–237.

Horner, T.J., Pryer, H.V., Nielsen, S.G., Crockford, P.W., Gauglitz, J.M., Wing, B.A., Ricketts, R.D., 2017. Pelagic barite precipitation at micromolar ambient sulfate. Nature Commun. 8 (1), 1342, Number: 1 Publisher: Nature Publishing Group.

Hsieh, Y.-T., Henderson, G.M., 2017. Barium stable isotopes in the global ocean: Tracer of Ba inputs and utilization. Earth Planet. Sci. Lett. 473, 269–278.

Hsieh, Y.-T., Paver, R., Tanzil, J.T.I., Bridgestock, L., Lee, J.N., Henderson, G.M., 2022. Multi-colony calibration of barium isotopes between shallow-water coral skeletons and in-situ seawater: Implications for paleo proxies. Earth Planet. Sci. Lett. 580, 117369.

Huang, F., Bai, R., Deng, G., Liu, X., Li, X., 2021. Barium isotope evidence for the role of magmatic fluids in the origin of Himalayan leucogranites. Sci. Bull. 66 (22), 2329–2336.

Ito, A., Wagai, R., 2017. Global distribution of clay-size minerals on land surface for biogeochemical and climatological studies. Sci. Data 4 (1), 170103, Number: 1 Publisher: Nature Publishing Group.

Kaushal, S.S., Likens, G.E., Pace, M.L., Reimer, J.E., Maas, C.M., Galella, J.G., Utz, R.M., Duan, S., Kryger, J.R., Yaculak, A.M., Boger, W.L., Bailey, N.W., Haq, S., Wood, K.L., Wessel, B.M., Park, C.E., Collison, D.C., Aisin, B.Y.I., Gedeon, T.M., Chaudhary, S.K., Widmer, J., Blackwood, C.R., Bolster, C.M., Devilbiss, M.L., Garrison, D.L., Halevi, S., Kese, G.Q., Quach, E.K., Rogelio, C.M.P., Tan, M.L., Wald, H.J.S., Woglo, S.A., 2021. Freshwater salinization syndrome: from emerging global problem to managing risks. Biogeochemistry 154 (2), 255–292.

Knight, A.C.G., Stevenson, E.I., Bridgestock, L., Jotautas Baronas, J., Knapp, W.J., Adhikari, B.R., Andermann, C., Tipper, E.T., 2024. The impact of adsorption–desorption reactions on the chemistry of Himalayan rivers and the quantification of silicate weathering rates. Earth Planet. Sci. Lett. 641, 118814.

Laird, D.A., Shang, C., 1997. Relationship between cation exchange selectivity and crystalline swelling in expanding 2:1 phyllosilicates. Clays Clay Miner. 45 (5), 681–689.

Li, Y.-H., Chan, L.-H., 1979. Desorption of Ba and226Ra from river-borne sediments in the Hudson estuary. Earth Planet. Sci. Lett. 43 (3), 343–350.

Li, W., Liu, X.-M., 2020. Experimental investigation of lithium isotope fractionation during kaolinite adsorption: Implications for chemical weathering. Geochim. Cosmochim. Acta 284, 156–172.

Li, W.-Y., Yu, H.-M., Xu, J., Halama, R., Bell, K., Nan, X.-Y., Huang, F., 2020. Barium isotopic composition of the mantle: Constraints from carbonatites. Geochim. Cosmochim. Acta 278, 235–243.

Liu, H.-C., Hsieh, J.-Y., Chen, Y.-H., You, C.-F., Jiang, W.-T., Wen, H.-Y., 2022. Adsorption and Desorption Behaviors of Sr on Montmorillonite: A Triple Sr Isotope Perspective. ACS Earth Space Chem. 6 (9), 2250–2260.

Lu, Y., Hu, S., Liang, Z., Zhu, M., Wang, Z., Wang, X., Liang, Y., Dang, Z., Shi, Z., 2020. Incorporation of Pb(II) into hematite during ferrihydrite transformation. Environ. Sci. Nano 7 (3), 829–841, Publisher: Royal Society of Chemistry.

Maher, K., 2011. The role of fluid residence time and topographic scales in determining chemical fluxes from landscapes. Earth Planet. Sci. Lett. 312 (1), 48–58.

Martin, R.T., 1980. Data handbook for clay materials and other non-metallic minerals. Clays Clay Miner. 28 (2), 160.

Martinez-Ruiz, F., Paytan, A., Gonzalez-Muñoz, M.T., Jroundi, F., Abad, M.M., Lam, P.J., Bishop, J.K.B., Horner, T.J., Morton, P.L., Kastner, M., 2019. Barite formation in the ocean: Origin of amorphous and crystalline precipitates. Chem. Geol. 511, 441–451.

Meybeck, M., 2003. 5.08 - Global occurrence of major elements in rivers. In: Holland, H.D., Turekian, K.K. (Eds.), Treatise on Geochemistry. Pergamon, Oxford, pp. 207–223.

Middleton, J.T., Hong, W.L., Paytan, A., Auro, M.E., Griffith, E.M., Horner, T.J., 2023a. Barium isotope fractionation in barite–fluid systems at chemical equilibrium. Chem. Geol. 627, 121453.

Middleton, J.T., Paytan, A., Auro, M., Saito, M.A., Horner, T.J., 2023b. Barium isotope signatures of barite–fluid ion exchange in equatorial Pacific sediments. Earth Planet. Sci. Lett. 612, 118150.

Milliman, J.D., Farnsworth, K.L., 2013. River discharge to the coastal ocean: a global synthesis. Cambridge University Press.

Misra, S., Froelich, P.N., 2012. Lithium isotope history of cenozoic seawater: Changes in silicate weathering and reverse weathering. Science 335 (6070), 818–823, Publisher: American Association for the Advancement of Science.

Moll, W.F., 2001. Baseline studies of the clay minerals society source clays: Geological origin. Clays Clay Miner. 49 (5), 374–380.

Nan, X., Wu, F., Zhang, Z., Hou, Z., Huang, F., Yu, H., 2015. High-precision barium isotope measurements by MC-ICP-MS. J. Anal. At. Spectrom. 30 (11), 2307–2315, Publisher: Royal Society of Chemistry.

Nan, X., Yu, H., Kang, J., Huang, F., 2022. Re-visiting barium isotope compositions of mid-ocean ridge basalts and the implications. Justc 52 (3), 1, Publisher: JUSTC.

Nan, X., Yu, H.-M., Rudnick, R.L., Gaschnig, R.M., Xu, J., Li, W.-Y., Zhang, Q., Jin, Z.-D., Li, X.-H., Huang, F., 2018. Barium isotopic composition of the upper continental crust. Geochim. Cosmochim. Acta 233, 33–49.

Nielsen, S.G., Horner, T.J., Pryer, H.V., Blusztajn, J., Shu, Y., Kurz, M.D., Le Roux, V., 2018. Barium isotope evidence for pervasive sediment recycling in the upper mantle. Sci. Adv. 4 (7), eaas8675.

Nielsen, S.G., Shu, Y., Auro, M., Yogodzinski, G., Shinjo, R., Plank, T., Kay, S.M., Horner, T.J., 2020. Barium isotope systematics of subduction zones. Geochim. Cosmochim. Acta 275, 1–18.

Pearce, C.R., Saldi, G.D., Schott, J., Oelkers, E.H., 2012. Isotopic fractionation during congruent dissolution, precipitation and at equilibrium: Evidence from Mg isotopes. Geochim. Cosmochim. Acta 92, 170–183.

Rudge, J.F., Reynolds, B.C., Bourdon, B., 2009. The double spike toolbox. Chem. Geol. 265 (3), 420–431.

Sajih, M., Bryan, N.D., Livens, F.R., Vaughan, D.J., Descostes, M., Phrommavanh, V., Nos, J., Morris, K., 2014. Adsorption of radium and barium on goethite and ferrihydrite: A kinetic and surface complexation modelling study. Geochim. Cosmochim. Acta 146, 150–163.

Sanders, C.J., Santos, I.R., Barcellos, R., Silva Filho, E.V., 2012. Elevated concentrations of dissolved Ba, Fe and Mn in a mangrove subterranean estuary: Consequence of sea level rise? Cont. Shelf Res. 43, 86–94.

Schroeder, P., 2018. Clays in the Critical Zone. Cambridge University Press.

Schroth, B.K., Sposito, G., 1997. Surface Charge Properties of Kaolinite. Clays Clay Miner. 45 (1), 85–91.

Schwertmann, U., Cornell, R.M., 2008. Iron oxides in the laboratory: preparation and characterization. John Wiley & Sons.

Sposito, G., Holtzclaw, K.M., Charlet, L., Jouany, C., Page, A.L., 1983. Sodium-calcium and sodium-magnesium exchange on wyoming bentonite in perchlorate and chloride background ionic media. Soil Sci. Soc. Am. J. 47 (1), 51–56.

Sposito, G., Skipper, N.T., Sutton, R., Park, S.-h., Soper, A.K., Greathouse, J.A., 1999. Surface geochemistry of the clay minerals. Proc. Natl. Acad. Sci. 96 (7), 3358–3364.

Sverjensky, D.A., 2006. Prediction of the speciation of alkaline earths adsorbed on mineral surfaces in salt solutions. Geochim. Cosmochim. Acta 70 (10), 2427–2453.

Tang, L., Sparks, D.L., 1993. Cation-exchange kinetics on montmorillonite using pressure-jump relaxation. Soil Sci. Soc. Amer. J. 57 (1), 42–46.

Teich-McGoldrick, S.L., Greathouse, J.A., Jové-Colón, C.F., Cygan, R.T., 2015. Swelling properties of montmorillonite and beidellite clay minerals from molecular simulation: Comparison of temperature, interlayer cation, and charge location effects. J. Phys. Chem. C 119 (36), 20880–20891, Publisher: American Chemical Society.

Teppen, B.J., Miller, D.M., 2006. Hydration energy determines isovalent cation exchange selectivity by clay minerals. Soil Sci. Soc. Am. J. 70 (1), 31–40.

Tieman, Z.G., Stewart, B.W., Capo, R.C., Phan, T.T., Lopano, C.L., Hakala, J.A., 2020. Barium isotopes track the source of dissolved solids in produced water from the unconventional marcellus shale gas play. Environ. Sci. Technol. 54 (7), 4275–4285.

Tipper, E.T., Stevenson, E.I., Alcock, V., Knight, A.C., Baronas, J.J., Hilton, R.G., Bickle, M.J., Larkin, C.S., Feng, L., Relph, K.E., Hughes, G., 2020. Global silicate weathering flux overestimated because of sediment-water cation exchange. Proc. Natl. Acad. Sci. USA 118 (1), Publisher: National Academy of Sciences.

Tournassat, C., Davis, J.A., Chiaberge, C., Grangeon, S., Bourg, I.C., 2016. Modeling the Acid–Base Properties of Montmorillonite Edge Surfaces. Environ. Sci. Technol. 50 (24), 13436–13445, Publisher: American Chemical Society.

van Zuilen, K., Harrison, A.L., Stammeier, J.A., Nagler, T.F., Mavromatis, V., 2023. Barium isotope (re-)equilibration in the barite-fluid system and its implications for marine barite archives. Earth Planet. Sci. Lett. 618, 118280.

van Zuilen, K., Müller, T., Nägler, T.F., Dietzel, M., Küsters, T., 2016. Experimental determination of barium isotope fractionation during diffusion and adsorption processes at low temperatures. Geochim. Cosmochim. Acta 186, 226–241.

von Allmen, K., Böttcher, M.E., Samankassou, E., Nägler, T.F., 2010. Barium isotope fractionation in the global barium cycle: First evidence from barium minerals and precipitation experiments. Chem. Geol. 277 (1), 70–77.

von Strandmann, P.A.P., Kasemann, S.A., Wimpenny, J.B., 2020. Lithium and lithium isotopes in earth's surface cycles. Elements 16 (4), 253–258.

Wei, W., Zeng, Z., Shen, J., Tian, L.-L., Wei, G.-Y., Ling, H.-F., Huang, F., 2021. Dramatic changes in the carbonate-hosted barium isotopic compositions in the ediacaran yangtze platform. Geochim. Cosmochim. Acta 299, 113–129.

White, A.F., Schulz, M.S., Stonestrom, D.A., Vivit, D.V., Fitzpatrick, J., Bullen, T.D., Maher, K., Blum, A.E., 2009. Chemical weathering of a marine terrace chronosequence, santa cruz, california. part II: Solute profiles, gradients and the comparisons of contemporary and long-term weathering rates. Geochim. Cosmochim. Acta 73 (10), 2769–2803.

Wu, F., Turner, S., Schaefer, B.F., 2020. Mélange versus fluid and melt enrichment of subarc mantle: A novel test using barium isotopes in the Tonga-Kermadec arc. Geology 48 (11), 1053–1057.

Yang, L., Steefel, C.I., 2008. Kaolinite dissolution and precipitation kinetics at 22 °C and pH 4. Geochim. Cosmochim. Acta 72 (1), 99–116.

Yu, Y., Hathorne, E., Siebert, C., Felis, T., Rajendran, C.P., Frank, M., 2022. Monthly resolved coral barium isotopes record increased riverine inputs during the South Asian summer monsoon. Geochim. Cosmochim. Acta 329, 152–167.

Zeebe, R.E., Wolf-Gladrow, D.A., Jansen, H., 1999. On the time required to establish chemical and isotopic equilibrium in the carbon dioxide system in seawater. Mar. Chem. 65 (3), 135–153.

Zhang, P.-C., Brady, P.V., Arthur, S.E., Zhou, W.-Q., Sawyer, D., Hesterberg, D.A., 2001. Adsorption of barium(II) on montmorillonite: an EXAFS study. Colloids Surf. A 190 (3), 239–249.

Zhao, Y.-P., Tang, Y.-J., Xu, J., Zeng, Z., Ying, J.-F., Tian, H.-C., Huang, F., 2021. Barium isotope evidence for recycled crustal materials in the mantle source of continental basalts. Lithos 390–391, 106111.